JGP Journal of General Physiology

RESEARCH ARTICLE

Heat-resistant action potentials require TTX-resistant sodium channels $Na_V1.8$ and $Na_V1.9$

Filip Touska[1,2], Brian Turnquist[3], Viktorie Vlachova[2], Peter W. Reeh[4], Andreas Leffler[5], and Katharina Zimmermann[1]

Damage-sensing nociceptors in the skin provide an indispensable protective function thanks to their specialized ability to detect and transmit hot temperatures that would block or inflict irreversible damage in other mammalian neurons. Here we show that the exceptional capacity of skin C-fiber nociceptors to encode noxiously hot temperatures depends on two tetrodotoxin (TTX)-resistant sodium channel α-subunits: $Na_V1.8$ and $Na_V1.9$. We demonstrate that $Na_V1.9$, which is commonly considered an amplifier of subthreshold depolarizations at 20°C, undergoes a large gain of function when temperatures rise to the pain threshold. We also show that this gain of function renders $Na_V1.9$ capable of generating action potentials with a clear inflection point and positive overshoot. In the skin, heat-resistant nociceptors appear as two distinct types with unique and possibly specialized features: one is blocked by TTX and relies on $Na_V1.9$, and the second type is insensitive to TTX and composed of both $Na_V1.8$ and $Na_V1.9$. Independent of rapidly gated TTX-sensitive Na_V channels that form the action potential at pain threshold, $Na_V1.8$ is required in all heat-resistant nociceptors to encode temperatures higher than ∼46°C, whereas $Na_V1.9$ is crucial for shaping the action potential upstroke and keeping the $Na_V1.8$ voltage threshold within reach.

Introduction

Environmental temperature acts as a strong evolutionary stressor. It affects multiple adaptive systems and, thereby, contributes to the shaping of the genomes and phenomes of all species (Nevo, 2011). For example, nervous systems of lower vertebrates and invertebrates are adapted to work best in temperatures from 0°C to 35°C. Between 36°C and 38°C, at which mammalian nerve cells are adapted to perform best, mollusk axons cease to conduct, because they suffer heat block (Hodgkin and Katz, 1949; Volgushev et al., 2000).

Apparently, changing temperature in either direction profoundly affects intrinsic and active properties of excitable membranes and synaptic activities (Volgushev et al., 2000). In rat neocortical cells, cooling leads to an increase in input resistance and a (near-linear) depolarization of the membrane potential. In addition, lowered potassium conductance of two-pore domain potassium (2PK)-channel subtypes decreases the total membrane conductance (Volgushev et al., 2000; Enyedi and Czirják, 2010). Therefore, in mammalian neocortical cells, temperatures between 18°C and 24°C create hyperexcitability, whereas at lower temperatures, cooling hinders repetitive firing, because it slows activation kinetics of sodium channels and also slows recovery from inactivation, in part by reducing the afterhyperpolarization (Volgushev et al., 2000). This was demonstrated to cause a reversible depolarization block in neocortical and hypothalamic neurons (Griffin and Boulant, 1995; Volgushev et al., 2000).

In cultured dorsal root ganglion (DRG) cells, tetrodotoxin-sensitive (TTXs) voltage-gated sodium channels are slowed with cooling and, at 10°C, become trapped in a state of slow inactivation (Zimmermann et al., 2007). In contrast to cortical neurons, the peripheral nociceptive terminals that innervate the skin with extended axons are specialized to detect temperature extremes that otherwise would produce tissue damage and pain. These nociceptors are equipped with several Na_V channel α-subunits that exhibit fast ($Na_V1.7$) or slow ($Na_V1.8$ and $Na_V1.9$) kinetics (Akopian et al., 1999; Dib-Hajj et al., 2002; Cox et al., 2006). The cold-sensitive subpopulations are endowed with the sodium channel α-subunit $Na_V1.8$ that serves as frost-resistant ignition and enables cold nociceptors to fire at high rates, even at low temperatures (Zimmermann et al., 2007).

Like cold nociceptors, heat-sensitive nociceptors must have endured a comparable specialized process of molecular adaptation of their sodium channel subtypes to ensure the detection and transmission of damaging heat. In the central nervous system (CNS), as was demonstrated with field potentials in (rabbit)

[1]Klinik für Anästhesiologie am Universitätsklinikum Erlangen, Friedrich-Alexander Universität Erlangen-Nürnberg, Erlangen, Germany; [2]Department of Cellular Neurophysiology, Institute of Physiology, Academy of Sciences of the Czech Republic, Prague, Czech Republic; [3]Department of Mathematics and Computer Science, Bethel University, St. Paul, MN; [4]Department of Physiology and Pathophysiology, Friedrich-Alexander-Universität Erlangen-Nürnberg, Erlangen, Germany; [5]Klinik für Anästhesiologie und Intensivmedizin, Medizinische Hochschule Hannover, Hannover, Germany.

Correspondence to Katharina Zimmermann: katharina.zimmermann@fau.de; Andreas Leffler: leffler.andreas@mh-hannover.de.

© 2018 Touska et al. This article is distributed under the terms of an Attribution–Noncommercial–Share Alike–No Mirror Sites license for the first six months after the publication date (see http://www.rupress.org/terms/). After six months it is available under a Creative Commons License (Attribution–Noncommercial–Share Alike 4.0 International license, as described at https://creativecommons.org/licenses/by-nc-sa/4.0/).

Downloaded from http://rupress.org/jgp/article-pdf/150/8/1125/1798734/jgp_201711786.pdf by guest on 09 February 2026

hippocampal slices, heating to 43°C leads to an irreversible loss of excitability (Shen and Schwartzkroin, 1988). In contrast, 42°C is the threshold for the heat response of cutaneous nociceptors, and the nerve endings and their cell bodies remain excitable at least until 50°C (Vyklický et al., 1999; Lyfenko et al., 2002; St Pierre et al., 2009; Zimmermann et al., 2009). To a certain extent, warming and heating seem to affect the membrane potential in the opposite direction from cooling (Volgushev et al., 2000); nevertheless, cellular recordings at temperatures >42°C, as tested for example in patch-clamped neurons from hippocampal slices, become less reliable and more unstable, and these effects are never completely reversible (Shen and Schwartzkroin, 1988). Therefore, the exact biophysical effects that lead to inactivation or a loss of excitability in central neurons above 43°C are unclear and extremely difficult to assess (Fujii and Ibata, 1982; Shen and Schwartzkroin, 1988); we hypothesize that, apart from irreversible changes to proteins, TTXs sodium channels may inactivate. How heat-sensitive nociceptors in the skin remain fully excitable, and are even able to fire at high rates when their receptive field is heated (Bessou and Perl, 1969), has never been addressed. In addition to the fast-gated $Na_V1.7$, the most abundant mammalian Na_V-channel subtypes in nociceptors are $Na_V1.8$ and $Na_V1.9$. Therefore, we hypothesize that molecular adaptation of sodium channel subtypes with slow kinetics imparts this evolutionarily indispensable capability.

Materials and methods

Animals

C57BL/6J, $Na_V1.8^{-/-}$, and $Na_V1.9^{-/-}$ mice weighing between 18 and 32 g were killed by 100% CO_2 and cervical dislocation. Animals were conventionally genotyped using commercially available primers (Metabion), as described in Zimmermann et al. (2007) and Ostman et al. (2008). $Na_V1.8^{-/-}$ and $Na_V1.9^{-/-}$ mice were a kind gift from John Wood (University College London, London, UK; Akopian et al., 1999; Ostman et al., 2008) and congenic to and mated with C57BL/6J (purchased from Charles River). Mice were housed in constant room temperature (22°C) and humidity between 40 and 60% under a 12-h light cycle and supplied with food and water ad libitum.

Nociceptor recordings

We used the isolated skin-saphenous nerve preparation and single-fiber recording technique together with DAPSYS software (Brian Turnquist; www.dapsys.net) and a DAP5200a/626 board (Microstar Laboratories), as previously described (Zimmermann et al., 2009). We recorded from preparations of C57BL/6J-based $Na_V1.8^{-/-}$, $Na_V1.9^{-/-}$, and littermate control mice. The skin was kept under laminar superfusion of carbogen-gassed synthetic interstitial fluid (SIF), pH 7.4, which contained (in mM) 108 NaCl, 3.48 KCl, 3.5 $MgSO_4$, 26 $NaHCO_3$, 11.7 NaH_2PO_4, 1.5 $CaCl_2$, 9.6 sodium gluconate, 5.55 glucose, and 7.6 sucrose (Bretag, 1969). Receptive fields of identified mechano-sensitive C-fibers were characterized with custom-designed gravity-driven von Frey filaments and with respect to thermal responsiveness (thermal stimuli were applied as a 20-s ramp-shaped stimulus from 30°C to 50°C or as 60-s stimulus, decreasing from 30°C to 5°C in a negative exponential shape). The criterion for assigning heat responsiveness to a fiber was a discharge of at least two spikes at ramp peak. The criterion for assigning cold responsiveness to a fiber was adjusted to a discharge of at least three spikes because of the longer cold ramp.

For thermal stimulation, the receptive fields were isolated from the surrounding fluid with a Teflon ring to reduce heat loss (inner diameter, 8 mm; volume, 300–400 µl) and were kept continuously perfused with SIF or TTX 1 µM at a rate of 10 ml/min, at controlled temperatures between 5°C and 50°C. To apply the solutions, we used a previously described custom-made countercurrent temperature exchange application system (Zimmermann et al., 2009). In brief, the temperature at the receptive field was in closest possible proximity to the application system's outlet (inner diameter, 1.5 mm). A 0.25-mm thin thermocouple wire (Omega) was placed at the orifice of the outlet, directly above the receptive field. Superfusion fluid was applied directly to the receptive field's surface, with the outlet placed at the spot of highest mechanosensitivity to avoid thermal gradients from the ring center, radially outwards.

For threshold tracking experiments, electrical stimulation was performed with the A395 linear stimulus isolator from WPI, controlled by our new feedback-regulated threshold tracking program (B. Turnquist). In brief, a high-impedance bipolar electrode with conical tip (Frederick Haer) was gently placed in the receptive field to softly touch the spot of highest mechanical sensitivity (without eliciting mechanically induced action potentials). Then the filter window was prepared to (1) select for the spike shape of interest and (2) select for the appropriate latency of the spike evoked by electrical stimulation. This ensures that mostly electrically evoked spikes are used to operate the feedback-controlled tracking algorithm; to account for temperature-induced slowing and speeding of the latency, a recognition time window for the latency was set to include ±70 ms. During tracking, each incoming spike in the filter window creates a digital trigger that operates the electrical stimulator. Incoming spikes trigger and set the current one unit lower for the next stimulus. Unsuccessful stimuli increase the next stimulus by one current unit. For tracking, Δ100 µA was used at a rate of 1/s, with a stimulus length between 0.5 and 2 ms (adjusted in each individual fiber). Before changing the temperature, the receptive field was kept at 30°C for at least 120 s to determine a constant basal electrical threshold for action potential excitation in each nociceptor. Excitability threshold at increasing and decreasing temperatures was then determined with a ramp-shaped stimulus, increasing at a rate of 0.07°C/s (± 0.02 SD) from 30°C to 50°C. Ramps lasted between 240 and 300 s. At any temperature at which the excitability was lost, the temperature was held at this particular value to allow the stimulus strength to gradually increase to reach the threshold again, or the threshold was manually increased by Δ1 mA until the fiber was found to be excitable again. Technically, fibers could be tracked up to 10 mA, the maximal range of the stimulator. Because the basal threshold was constant in each nociceptor recording, but variable between fibers, thresholds were normalized to the basal threshold for statistical analysis (compare Figs. 10 C and 12 C). This proceeding entails an error for the data points at which fibers were not excitable within

Downloaded from http://rupress.org/jgp/article-pdf/150/8/1125/1798734/jgp_201711786.pdf by guest on 09 February 2026

stimulator range. Therefore, the results presented in the main text mention the mean temperature at which the last spike was recorded. If possible, the excitability range for all temperatures was also measured after application of 1 µM TTX.

The frequency plots were calculated from averaging firing rates per °C and subjecting the data to a three-point averaging procedure. If possible, slopes were calculated from linear fits of the data points >0.01/s from the first positive increase to the data point with the maximum difference between adjacent data points.

DRGs

DRG neurons were isolated from all spinal levels of adult mice of the C57BL/6J, $Na_V1.8^{-/-}$, and $Na_V1.9^{-/-}$ strains, killed by CO_2. Neurons were collected in 0.6 mg/ml collagenase (type XI, Sigma-Aldrich) and 3 mg/ml protease (Sigma-Aldrich) for 40 min at 37°C in DMEM. Cells were washed three times, triturated, and plated on poly-D-lysine (0.1 mg/ml) borosilicate glass coverslips in serum-free TNB-100 basal medium (Biochrom), supplemented with penicillin, streptomycin, and 100 ng/ml nerve growth factor-7S (Alomone Labs). Recordings were performed between 3 and 24 h after dissection. In contrast to others, we have not used low-temperature incubation to increase the functional expression of $Na_V1.9$ (Vanoye et al., 2013; Leipold et al., 2015). As in our previous studies, we kept the plated DRGs in an incubator at 37°C to obtain acceptable patch-clamp conditions for sensory neurons.

N1E-115 and ND7/23 cells

Both cell lines were cultured at 37°C in 5% CO_2 in DMEM (Gibco; Thermo Fisher Scientific) supplemented with 5 g/liter glucose, 10% FBS (Biochrom), and 1% penicillin/streptomycin (Biochrom).

Patch-clamp recordings

Whole-cell patch-clamp recordings were conducted with an Axopatch 200B amplifier/Clampex 10.4 software (Molecular Devices) or EPC 10USB/Patchmaster software (HEKA Elektronik). Glass pipettes were fabricated with a P-1000 Micropipette Puller (Sutter), with 1.8–3-MΩ resistance for voltage-clamp configuration and 3.5–6-MΩ resistance for current-clamp configuration. The bath solution contained (in mM) 140 NaCl, 3 KCl, 1 $CaCl_2$, 1 $MgCl_2$, 10 HEPES, 20 glucose, and 0.1 $CdCl_2$, adjusted to pH 7.4 with NaOH. In Fig. 5 B ($Na_V1.8$ inactivation time constant), external sodium was reduced to 70 mM with 70 mM choline chloride. For voltage-clamp recordings, 20 mM TEA-Cl was added. Pipette solution for voltage-clamp recordings contained (in mM) 120 CsCl, 10 NaCl, 10 HEPES, 10 EGTA, 2.2 $MgCl_2$, 1.9 $CaCl_2$, 5 TEA-Cl, 4 MgATP, and 0.2 Na_2GTP, pH 7.3, adjusted with CsOH. CsF-based pipette solution contained (in mM) 140 CsF, 10 NaCl, 10 HEPES, 1 EGTA, and 5 TEA-Cl, pH 7.3 with NaOH, and was also used for voltage-clamp experiments with N1E-115 and ND7/23 cells and for assessing $Na_V1.8$ inactivation time constant (Fig. 5 B). 500 or 1,500 nM TTX was added as indicated. The pipette solution for current-clamp recordings contained (in mM) 135 potassium gluconate, 4 NaCl, 3 $MgCl_2$, 0.3 Na-GTP, 2 Na_2-ATP, 5 EGTA, and 5 HEPES, adjusted to pH 7.3 with KOH. Currents were sampled at the rate of 20–100 kHz, based on the protocol type. Series resistance was compensated for (65–85%). For voltage-clamp recordings, the holding potential was −90 mV. To normalize current-clamp recordings and prevent all sodium channel isoforms from inactivation, the membrane potential was set to approximately −80 mV by injecting current; incrementing current pulses were injected until the action potential threshold was reached. Voltage dependence of activation was measured using 500-ms voltage pulses from a holding potential of −90 mV, with 10-mV increments up to +30 mV for presumptive $Na_V1.9$ currents or +50 mV for presumptive $Na_V1.8$ currents. Conductance was derived from activation curves using the following equation:

$$G_{Na} = \frac{I_{Na}}{V_m - E_{rev}},$$

where I_{Na} is the peak current amplitude, V_m is the actual voltage pulse, and E_{rev} is the reversal potential calculated for each current pulse. For comparison of the voltage of half-maximal activation, the data were least-squares-fitted by using a Boltzmann fit according to the following equation:

$$G_{Na} = \frac{G_{max}}{1 + e^{\frac{V_{1/2} - V_m}{k}}},$$

where G_{max} is the maximum sodium conductance, $V_{1/2}$ is the membrane potential at half-maximal activation, V_m is the membrane voltage, and k is the slope factor. Action potential voltage threshold was measured as the value of the inflection point, where the rising phase of the action potential clearly deviated from the passive response and was fitted with a single or double exponential curve.

To control the superfusion temperature, we used a gravity-driven perfusion system, where the temperature was adjusted as described previously (Dittert et al., 2006). For voltage- and current-clamp experiments, single DRGs were measured at three different temperatures (starting at 20°C, followed by 10°C and 30°C or 20°C, followed by 37°C and 43°C, respectively) 3–8 min after establishing the whole-cell mode. For voltage-clamp experiments, in each group at least three cells were tested by changing the order of temperature application (first applying 30°C or 43°C and then 10°C or 20°C) or measuring one consecutive activation protocol at 20°C at the end of the protocol to ensure that the increase in current density observed for presumptive $Na_V1.9$ currents (measured in DRGs derived from $Na_V1.8$-deficient mice with TTX and either CsCl or CsF in the pipette) were reversible and caused by the temperature change. During voltage-clamp experiments with CsF, we observed a continuous increase in current amplitude followed by a decrease of the current, similar to the description of previous authors (Rugiero et al., 2003; Coste et al., 2004). This effect is apparent in Fig. 2 (E and F) and Fig. 4 C; however, we found no systematic influence on the observed temperature-induced effects.

Animal behavior

The protocol for in vivo experiments in animals was reviewed by the local animal ethics committee (University of Erlangen) and approved by the local district government. Experiments involving live animals were conducted in accordance with the International Association for the Study of Pain Guidelines for the Use of Animals in Research. Mice were anesthetized with sevoflurane

Downloaded from http://rupress.org/jgp/article-pdf/150/8/1125/1798734/jgp_201711786.pdf by guest on 09 February 2026

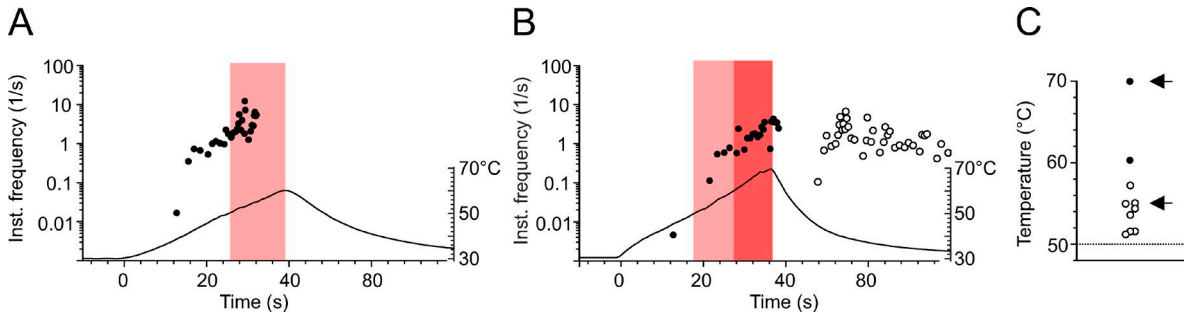

Figure 1. **Cutaneous polymodal nociceptors are heat resistant, and some encode up to 70°C. (A and B)** Original recordings from two polymodal nociceptors innervating receptive fields in mouse saphenous-nerve innervated skin. Instantaneous discharge rates in response to superfusion heating of the receptive field are shown. Each circle represents one action potential. Heat stimuli were ramp-shaped and are plotted as a temperature time course, with the temperature scale indicated on the right. The light and dark red bars mark action potentials discharged above 50°C or 60°C, respectively. **(A)** Ramp-shaped heating at a rate of 0.75°C/s from 30°C to 60°C. The fiber encodes the temperature until 55°C before it ceases to discharge. **(B)** Ramp-shaped heating at a rate of 1°C/s; the fiber encodes the temperature until 70°C, but after the stimulus, nerve and receptive field are left with ongoing activity at 32°C. **(C)** 10 mouse polymodal nociceptors were subjected to ramp-shaped heating from 30° to at least 60°C. The temperature of the last action potential in response to heating is given. Most fibers inactivate between 50°C and 60°C (white circles; $n = 8$). Some nociceptors encode >60°C ($n = 2$; black circles). The arrows mark the original recordings illustrated in A and B.

and injected with TTX (20 µl, 3 µM) intracutaneously in the plantar hindpaw skin. Mice were placed in an acrylic glass chamber with a Kevlar grid surface. The Hargreaves infrared probe (Ugo Basile) was placed under the plantar surface, and the latency was automatically recorded as soon as the mouse withdrew. Cutoff time of the heat pulse was set to 30 s to avoid tissue damage. Mice were habituated 1 d before the experiment and also 1 h before the first measurement. Paw withdrawal latency was measured 4–10 min after the mouse had received the TTX injection and had regained consciousness. TTX effects lasted for maximum 10 min. Eight mice per genotype were measured, and at least two consecutive measurements were performed on the same hindpaw with minimal time difference of 3 min and maximal of 6 min between measurements. Values measured on the same hindpaw were averaged. The measurements were repeated with the same mouse groups after 5 d, and TTX was applied on the contralateral side. The experimenter was blinded to the genotype and injection.

Data analysis and statistics

Patch-clamp electrophysiological data were analyzed using Clampfit 10 (Molecular Devices), HEKA Fitmaster (HEKA Elektronik), and Igor Pro 5.2–6.0 (Wavemetrics) with NeuroMatic and custom-build (Hampl et al., 2016) extensions. Origin 8.5 and Corel Draw X6 were used for graphical interpretation. Data are depicted as means ± SEM if not otherwise indicated. Student's paired and unpaired *t* test, ANOVA followed by Tukey's honestly significant difference (HSD) post hoc test, or Mann–Whitney *U* test were used where appropriate and calculated with Statistica 6 (formerly StatSoft) and SPSS (IBM) v.21 when not otherwise indicated. Significance is indicated in figures with asterisks: *, $P < 0.05$; **, $P < 0.01$; and ***, $P < 0.001$.

Results

Dynamic range of high temperature encoding in nociceptors

When receptive fields of heat-sensitive nociceptors in the skin are exposed to noxious heat, they encode and transmit the information to the CNS. In isolated skin-nerve preparations, rat and mouse nociceptors can repeatedly respond to a 50°C heat stimulus (St Pierre et al., 2009; Zimmermann et al., 2009) with propagated action potentials, but most polymodals undergo conduction block between 50°C and 60°C (Fig. 1, A and C, white circles). Some nociceptors (2 of 10) seem capable of encoding higher temperatures between 60°C and 70°C once and for a few seconds without suffering inactivation (Fig. 1, B and C). After 70°C exposure, the skin suffers visible burn damage, and nociceptors may be destroyed or left with ongoing injury discharge when the skin temperature returns to ambient temperature (Fig. 1 B). To identify the particular subtypes of Na_V channels that are essential for electrogenesis at high temperatures, we used whole-cell recordings from dissociated DRG neurons, the cell bodies of the skin nociceptors.

Rising temperatures raise the $Na_V1.9$ current more than any other Na_V current

Using the voltage-clamp configuration, we found that especially TTX-resistant (TTXr) currents undergo a remarkable speeding of their kinetics with heating. The speeding of the sodium current activation kinetics was profound in one particular subgroup of small-diameter DRG neurons (<27 µm) that were derived from $Na_V1.8^{-/-}$ animals and measured in the presence of 500 nM TTX in the extracellular solution (Fig. 2 A, left). The sodium current in this subgroup showed the typical attributes of $Na_V1.9$ with slow activation kinetics and persistent current (Tate et al., 1998; Cummins et al., 1999; Dib-Hajj et al., 2002). In addition, this current was clearly distinguishable from the current produced by $Na_V1.8$, which activates at more positive voltage values and shows a faster kinetic of activation and inactivation (Fig. 2 C, left). The midpoints of activation ($V_{1/2}$) values (determined by a Boltzmann fit) for presumed $Na_V1.8$ current assessed in $Na_V1.9^{-/-}$ DRGs in the presence of 500 nM TTX were −16 ± 2 mV at 20°C, −12 ± 1 mV at 30°C, and −19 ± 1 mV at 10°C ($n = 5$, $P = 0.02$). For $Na_V1.9$-like currents of $Na_V1.8^{-/-}$ neurons, the corresponding values were −33 ± 2 mV at 20°C and −29 ± 1 mV at 30°C ($n = 6$, $P = 0.02$). At 10°C, the amplitude of the peak current was too small and the kinetics of $Na_V1.9$ too slow to be quantified.

Downloaded from http://rupress.org/jgp/article-pdf/150/8/1125/1798734/jgp_201711786.pdf by guest on 09 February 2026

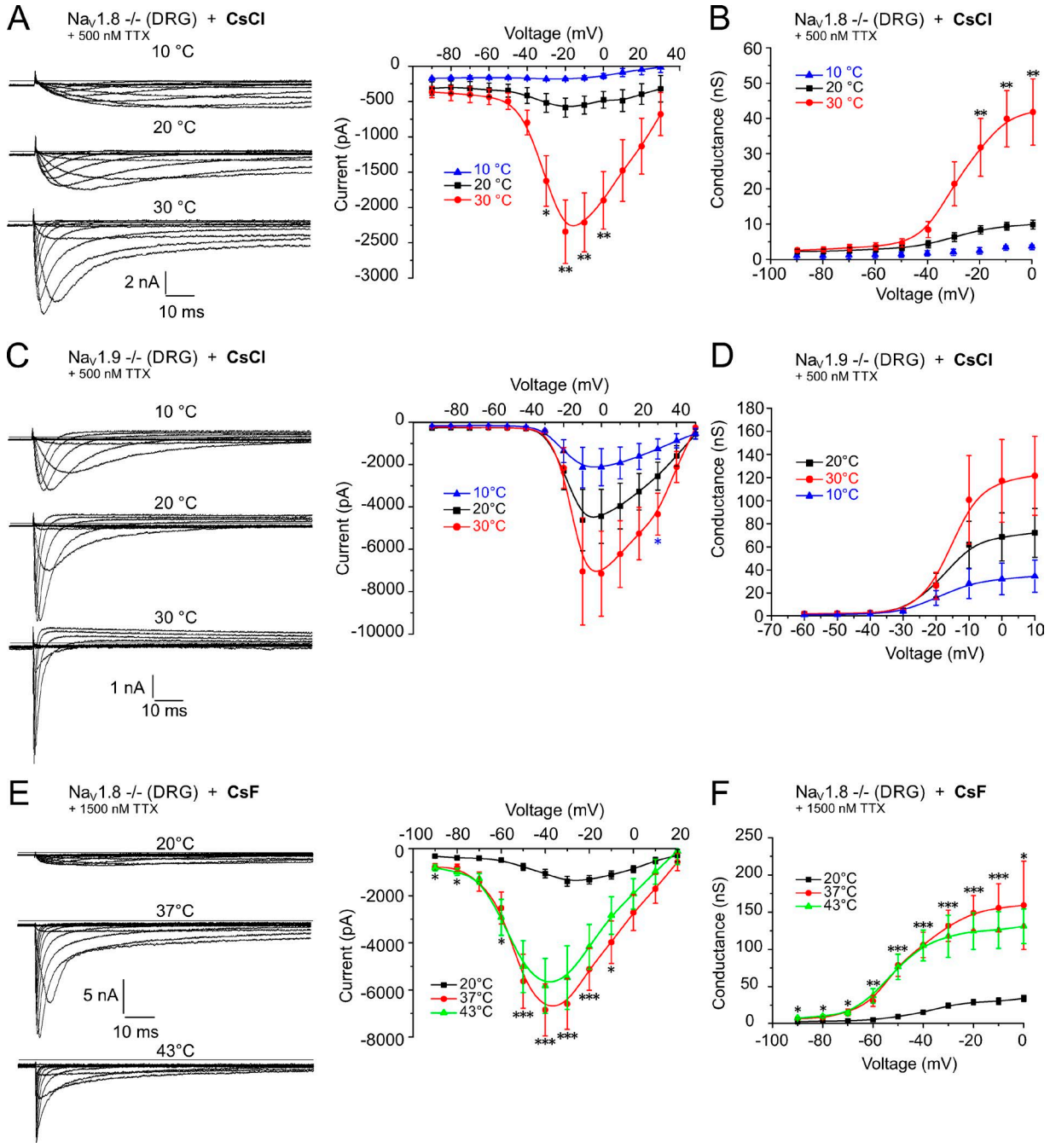

Figure 2. **$Na_V1.9$ undergoes a larger warming-induced gain of function than $Na_V1.8$.** Neurons were held at −90 mV and stimulated with 500-ms voltage pulses from −90 mV up to +50 mV. **(A, C, and E, left panels)** Sample traces of the specific voltage-gated sodium currents at three indicated temperatures. **(A, C, and E, right panels; and B, D, and F)** The effect of temperature on the voltage-dependence of activation and the conductance, respectively. **(A–D)** Presumptive $Na_V1.9$ current from a cultured small-diameter $Na_V1.8^{-/-}$ DRG (A and B) and $Na_V1.8$ current from a $Na_V1.9^{-/-}$ DRG (C and D), both recorded in the presence of 500 nM TTX with a CsCl-based pipette solution at 10°C, 20°C, and 30°C. An increase in temperature from 20°C to 30°C enlarged the $Na_V1.9$ (CsCl) peak current amplitude 4.0-fold (−585.8 ± 135.7 pA, n = 9, to −2,342.8 ± 448.8 pA, n = 8, P = 0.002) and the conductance 3.8-fold (8.3 ± 1.2 nS, n = 8, to 31.5 ± 8.1 nS, n = 6, P = 0.006). In contrast, the $Na_V1.8$ peak current amplitude increased 1.6-fold (−4,444.3 ± 1,275.6 to −7,147.6 ± 2,005.5 pA, n = 8) and the conductance 1.7-fold (68.6 ± 20.8 to 117.1 ± 35.8 nS, n = 8, P > 0.05). **(E and F)** Presumptive $Na_V1.9$ current from small-diameter $Na_V1.8^{-/-}$ DRG, acquired with a CsF-based pipette solution and in the presence of 1,500 nM TTX at 20°C, 37°C, and 43°C, showed a 4.9-fold increase in the peak current amplitude at 37°C compared with 20°C (−1,388.7 ± 208.2 pA, n = 15, to −6,844.0 ± 1,108.4 pA, n = 17, P = 0.0001) and a 4.3-fold increase in the conductance (24.5 ± 3.4 nS, n = 15, to 106.1 ± 17.1 nS, n = 16, P = 0.0003). At 43°C, peak current and conductance were not significantly different from 37°C. Data are depicted as means ± SEM. *, P < 0.05; **, P < 0.01; and ***, P < 0.001 (one-way ANOVA with Tukey HSD).

For $Na_V1.9$, increasing the temperature from 20°C to 30°C had a large impact on the speeding of activation and inactivation, and induced a large increase (4.0-fold) in the peak current (−585.8 ± 135.7 pA, n = 9, to −2,342.8 ± 448.8 pA, n = 8, P = 0.002; Fig. 2 A, right) and a similar increase (3.8-fold) in the conductance (8.3 ± 1.2 nS, n = 8, to 31.5 ± 8.1 nS, n = 6, P = 0.006; Fig. 2 B). Although the

Downloaded from http://rupress.org/jgp/article-pdf/150/8/1125/1798734/jgp_201711786.pdf by guest on 09 February 2026

Table 1. **Summary of electrophysiological parameters determined for TTXr sodium channels $Na_V1.9$ and $Na_V1.8$.** Parameters were measured in DRGs isolated from $Na_V1.8$- or $Na_V1.9$-deficient mice in the presence of 500 nM TTX and at 10°C, 20°C, and 30°C

Channel	Peak current (pA)				Conductance (nS)				Integrated peak area (pA)				Inactivation time constant (ms)			Time to peak (ms)			
	10°C	20°C	30°C	FC	10°C	20°C	30°C	FC	10°C	20°C	30°C	FC	20°C	30°C	FC	10°C	20°C	30°C	FC
$Na_V1.9$		−585.8 ± 135.7	−2,342.8 ± 448.7	**4.0**		8.3 ± 1.2	31.5 ± 8.1	**3.8**		4.9 ± 1.3	22.0 ± 6.8	**4.5**	31.0 ± 9.1	8.0 ± 1.2	**3.9**	40.7 ± 11.2	12.2 ± 1.9	3.5 ± 0.5	**3.3, 3.5**
$Na_V1.8$	−2,120 ± 876.8	−4,444.3 ± 1,275.6	−7,147.6 ± 2,005.5	**1.6**	32.2 ± 13.7	68.6 ± 20.8	117.1 ± 35.8	**1.7**	9.7 ± 3.2	15.7 ± 4.9	13.8 ± 4.2	**0.9**	2.5 ± 0.3	0.9 ± 0.1	**2.8**	6.4 ± 0.3	2.9 ± 0.2	1.3 ± 0.1	**2.2, 2.2**

All recordings were made with CsCl in the pipette solution. FC, fold change comparing 30°C with 20°C.

Table 2. **Summary of electrophysiological parameters determined for the TTXr sodium channel $Na_V1.9$ and TTXs sodium channel subtypes.** The parameters were measured in DRGs isolated from $Na_V1.8$-deficient mice in the presence of 1,500 nM TTX and in the ND7/23 and N1E-115 cell lines

Current	Peak current (pA)				Conductance (nS)				Integrated peak area (pA)				Time to peak (ms)			
	20°C	37°C	43°C	FC	20°C	37°C	43°C	FC	20°C	37°C	43°C	FC	20°C	37°C	43°C	FC
$Na_V1.9$	−1,388.7 ± 208.2	−6,844 ± 1,108.4	−5,828.9 ± 1,168.5	**4.9, 4.2**	24.5 ± 3.4	106.1 ± 17.1	105.2 ± 20.5	**4.3, 4.3**	9.4 ± 1.5	43.5 ± 6.7	30.5 ± 4.8	**4.6, 3.2**	34.6 ± 5.0	2.4 ± 0.3	1.1 ± 0.1	**14.4, 31.5**
TTXs in ND7/23	−2,335.0 ± 302.0	−2,314.1 ± 344.0	−1,605.4 ± 151.0	**1.0, 0.7**	37.1 ± 5.1	37.6 ± 5.7	25.0 ± 5.0	**1.0, 0.7**	2.0 ± 0.2	0.6 ± 0.1	0.4 ± 0.1	**0.3, 0.2**	0.58 ± 0.03	0.24 ± 0.02	0.19 ± 0.01	**2.4, 3.1**
TTXs in N1E-115	−3,210.0 ± 310.6	−3,776.0 ± 294.8	−2,350.0 ± 296.6	**1.2, 0.7**	46.9 ± 5.7	58.9 ± 6.5	30.1 ± 6.7	**1.3, 0.6**	4.4 ± 0.4	2.6 ± 0.2	1.5 ± 0.1	**0.6, 0.3**	0.79 ± 0.05	0.37 ± 0.03	0.30 ± 0.03	**2.1, 2.6**

All recordings were made with CsF in the pipette solution at 20°C, 37°C, and 43°C. FC, fold change comparing 37°C and 43°C with 20°C.

peak current conductance at 30°C is higher for $Na_V1.8$ compared with $Na_V1.9$ (117.1 ± 35.8 nS for $Na_V1.8$ vs. 31.5 ± 8.1 nS for $Na_V1.9$; Fig. 2, C and D), the potentiating effect of the 10°C temperature rise from 20°C to 30°C was much smaller on $Na_V1.8$, where the peak current amplitude increased 1.6-fold (from −4,444.3 ± 1,275.6 to −7,147.6 ± 2,005.5 pA, n = 8, P > 0.05) and the conductance 1.7-fold (from 68.6 ± 20.8 to 117.1 ± 35.8 nS, n = 8, P > 0.05) at the indicated voltages (Fig. 2, A and C, right; Fig. 2, B and D; and Table 1).

Next, we measured the sodium current activation at higher temperatures and compared the effect of 20°C, 37°C, and 43°C in the same cell. In contrast to previous experiments, we used a fluoride-based (CsF) and not chloride-based (CsCl) intracellular solution. Fluoride induces a leftward shift of the voltage dependence of activation in $Na_V1.9$ and potentiates the current amplitude (Rugiero et al., 2003; Coste et al., 2004). Fluoride also facilitates seal formation and improves seal stability, which is desirable for measurements at higher temperature. The sodium peak current, apparently from $Na_V1.9$ (derived from $Na_V1.8$-deficient neurons with 1,500 µM TTX), increased from −1,388.7 ± 208.2 pA, n = 15, at 20°C to −6,844.0 ± 1,108.4 pA, n = 17, at 37°C and −5,828.9 ± 1,168.5 pA, n = 9, at 43°C. Compared with 20°C, this represents a 4.9-fold increase at 37°C (P < 0.0001) and a 4.2-fold increase at 43°C (P = 0.005; Fig. 2 E, right). The conductance at peak current changed from 24.5 ± 3.4 nS (20°C, n = 15) to 106.1 ± 17.1 nS (37°C, n = 16, 4.3-fold) and 105.2 ± 20.6 nS (43°C, n = 9, 4.3-fold; P = 0.0003 between 20°C and 37°C and P = 0.002 between 20°C and 43°C; Fig. 2 F and Table 2).

To obtain a quantification of the effect of high temperatures on the TTXs currents, we measured the native TTXs currents in rodent neuroblastoma cell lines ND7/23 and N1E-115 (Fig. 3). These cell lines are not equivalent to the physiological environment and the particular Na_V channel subtypes present in DRG neurons, because they predominantly express $Na_V1.7$ and $Na_V1.6$ (ND7/23; Rogers et al., 2016) and $Na_V1.3$ (N1E-115; Jo and Bean, 2011) and are devoid of TTXr subtypes, but they allow insight into the effects of high temperature on the isolated TTXs current component, which is complicated to achieve in DRGs.

In ND7/23 cells, the TTXs peak current amplitude (0 mV) remained almost unchanged at 20°C and 37°C, and was −2,335.0 ± 302 pA (20°C) and −2,314.1 ± 344 pA (37°C), respectively (n = 20). Between 20°C and 43°C, the peak current amplitude decreased to −1,605.4 ± 151 pA (n = 20, 0.7-fold; Fig. 3 A). The peak current conductance was 37.1 ± 5.1 nS at 20°C, n = 20, and remained unchanged at 37°C (37.6 ± 5.7 nS, n = 17) and decreased to 25.0 ± 5.0 nS at 45°C, n = 16 (0.7-fold change; Fig. 3 B).

In N1E-115 cells, the peak current amplitude increased 1.2-fold, from −3,210.0 ± 310.6 pA (20°C) to −3,776.0 ± 294.8 pA (37°C), and then decreased to −2,350.0 ± 296.6 pA at 43°C (n = 10, 0.7-fold, P = 0.047 for peak current amplitude between 37°C and 43°C; Fig. 3 C). The peak current conductance changed 1.3-fold, from 46.9 ± 5.7 nS (n = 10, 20°C) to 58.9 ± 6.5 nS (n = 10, 37°C) and was reduced to 30.1 ± 6.7 nS at 43°C (n = 9, 0.6-fold, P = 0.01 between 37°C and 43°C; Fig. 3 D and Table 2). Apparently, when temperatures rise to the heat threshold, TTXs currents undergo

Downloaded from http://rupress.org/jgp/article-pdf/150/8/1125/1798734/jgp_201711786.pdf by guest on 09 February 2026

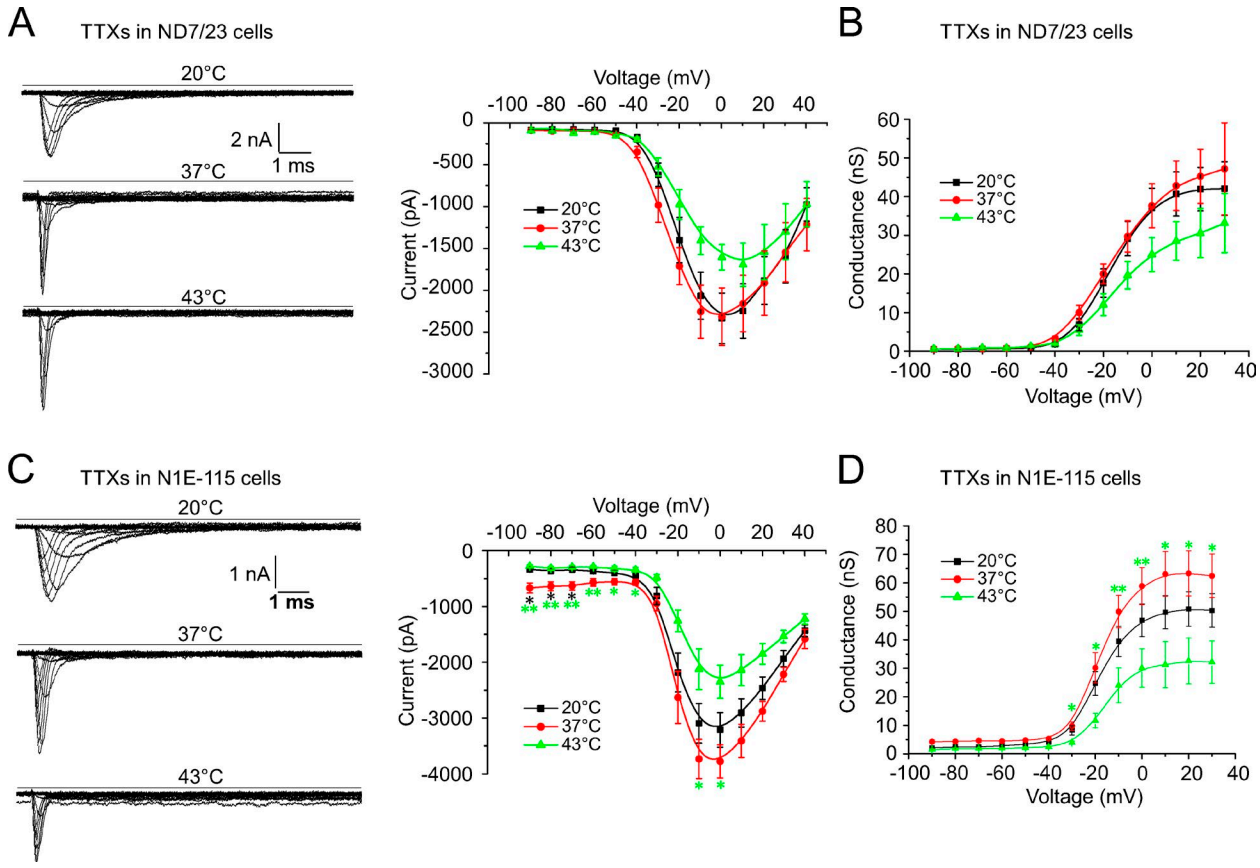

Figure 3. **Warming reduces TTXs native sodium currents recorded from ND7/23 and N1E-115 cells.** Cells were voltage-clamped at −90 mV and stimulated with 100-ms voltage pulses from −90 mV up to +40 mV using a CsF-based pipette solution. **(A and C, left panels)** Sample traces of the TTXs currents in ND7/23 (A) and N1E-115 (C) cells at three indicated temperatures. **(A and C, right panels; and B and D)** The effect of temperature on the voltage-dependence of activation and the conductance, respectively. **(A and B)** In ND7/23 cells, the TTXs peak current amplitude remained unchanged between 20°C and 37°C (−2,335.0 ± 302 pA, *n* = 20, to −2,314.1 ± 344 pA, *n* = 20) and decreased at 43°C (−1,605.4 ± 151 pA, *n* = 16). The effect of the temperature increase on the peak current conductance was similar (37.1 ± 5.1 nS at 20°C, *n* = 20; 37.6 ± 5.7 nS at 37°C, *n* = 17; and 25.0 ± 5.0 nS at 43°C, *n* = 16). **(C and D)** In N1E-115 cells, the TTXs peak current amplitude increased slightly between 20°C and 37°C (−3,210.0 ± 310.6 to −3,776.0 ± 294.8 pA) and decreased at 43°C (−2,350.0 ± 296.6 pA, *n* = 10, P = 0.047 between 37°C and 43°C). The effect of the temperature increase on the peak current conductance was similar (46.9 ± 5.7 nS at 20°C, *n* = 10; 58.9 ± 6.5 nS at 37°C, *n* = 10; and 30.1 ± 6.7 nS at 43°C, *n* = 9, P = 0.01 between 37°C and 43°C). Data are depicted as means ± SEM. *, P < 0.05; **, P < 0.01; and ***, P < 0.001 (one-way ANOVA with Tukey HSD).

a decline of their peak current and $Na_V1.9$ reaches a maximum of its peak current and conductance and then remains relatively constant.

Next, we calculated the integrated peak current (area under the curve [AUC]) of the sodium current from the entire peak current including the inactivation component, but excluding the persistent current. This quantifies the amount of sodium ions fluxing across the respective Na_V channel subtypes at each voltage (Fig. 4). At 30°C, compared with 20°C, the $Na_V1.9$ currents underwent a large, temperature-induced increase from 4.9 ± 1.3 to 22.0 ± 6.8 pA (*n* = 7, at −20 mV, P = 0.025; Fig. 4 A); this represented a 4.5-fold increase of the AUC at the voltage of the maximal peak current. In contrast, the amount of current for $Na_V1.8$ ($Na_V1.9$-deficient neurons with 500 µM TTX in the bath and CsCl in the pipette solution) remained constant over the entire temperature range (0.9-fold at the voltage of the maximal peak current; Fig. 4 B and Table 1). The respective integrated peak current was 15.7 ± 4.9 pA at 20°C, 13.8 ± 4.2 at 30°C, and 9.7 ± 3.2 at 10°C (*n* = 8, P > 0.05; Fig. 4 B). At higher temperatures, the maximal integrated peak area for $Na_V1.8$-deficient neurons with 1,500 µM TTX in the bath and CsF in the pipette solution changed 4.6-fold, from 9.4 ± 1.5 pA at 20°C, *n* = 16, to 43.5 ± 6.7 pA at 37°C, *n* = 18, and was 3.2-fold changed to 30.5 ± 4.8 pA, *n* = 11, at 43°C (P < 0.0001 between 20°C and 37°C, P = 0.026 between 20°C and 43°C; Fig. 4 C and Table 2). These findings indicate an increasing contribution of $Na_V1.9$ to the action potential current when temperatures rise.

In contrast, the integrated peak current area of the TTXs current of ND7/23 cells was reduced from 2.0 ± 0.2 pA, *n* = 24, at 20°C to 0.6 ± 0.1 pA, *n* = 21, at 37°C (0.3-fold, P < 0.0001) and appeared further reduced to 0.4 ± 0.1 pA, *n* = 21, at 43°C (0.2-fold, P < 0.0001; Fig. 4 D). Similar results were obtained for the N1E-115 cell line, where the maximal integrated peak area decreased from 4.4 ± 0.4 pA at 20°C to 2.6 ± 0.2 pA at 37°C, and to 1.5 ± 0.1 pA at 43°C (*n* = 10, P < 0.0001 between 20°C and 43°C, P = 0.018 between 37°C and 43°C; Fig. 4 E and Table 2).

To quantify the effect of temperature on the speeding of the inactivation kinetics, we calculated the inactivation time

Downloaded from http://rupress.org/jgp/article-pdf/150/8/1125/1798734/jgp_201711786.pdf by guest on 09 February 2026

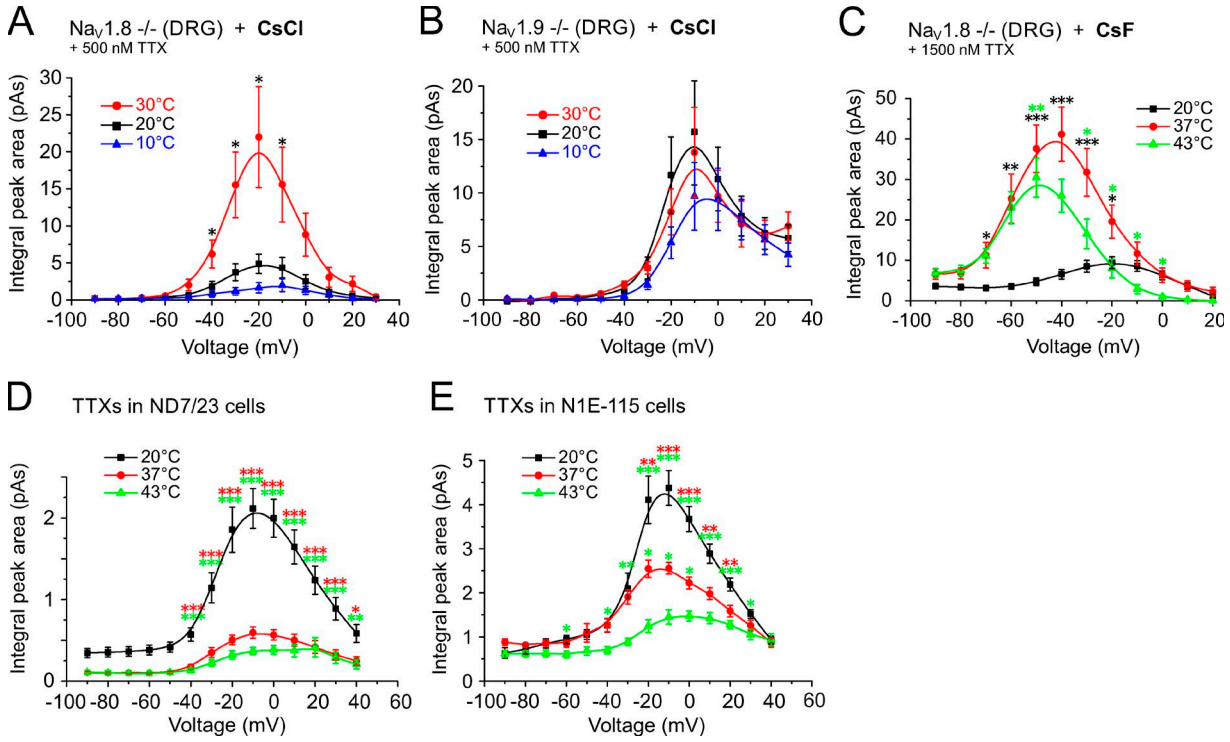

Figure 4. **Warming increases current density of $Na_V1.9$ more than that of $Na_V1.8$ or TTXs.** Shown are the measurements of the integrated peak current area for each voltage pulse (including the inactivation component and excluding the persistent current) at three indicated temperatures. Neurons were held at −90 mV and stimulated with 500-ms voltage pulses from −90 mV up to +50 mV. In A and B, recordings were obtained in the presence of 500 nM TTX using a CsCl-based pipette solution; in C, 1,500 nM TTX; and in C–E, a CsF-based pipette solution was used. **(A)** The current density of putative $Na_V1.9$ recorded from cultured small-diameter $Na_V1.8^{-/-}$ DRGs increased from 4.9 ± 1.3 pA at 20°C to 22.0 ± 6.8 pA at 30°C (at −20 mV, n = 7, P= 0.025). **(B)** The $Na_V1.8$ current density recorded from $Na_V1.9$-deficient DRGs remained largely unchanged and was 15.7 ± 4.9 pA at 20°C, 13.8 ± 4.2 at 30°C, and 9.7 ± 3.2 at 10°C (n = 8, P > 0.05). **(C)** At higher temperatures, the current density of the putative $Na_V1.9$ current increased from 9.4 ± 1.5 pA at 20°C, n = 16, to 43.5 ± 6.7 pA at 37°C, n = 18, and to 30.5 ± 4.8 pA at 43°C, n = 11; P < 0.0001 between 20°C and 37°C and P = 0.026 between 20°C and 43°C). **(D)** The integrated peak current area of the TTXs sodium currents recorded from ND7/23 were reduced from 2.0 ± 0.2 pA, n = 24, at 37°C to 0.6 ± 0.1 pA, n = 21, at 20°C (P = 0.0001) and to 0.4 ± 0.1 pA, n = 21, at 43°C (P < 0.0001). **(E)** Similarly, the integrated peak current area of the TTXs sodium currents recorded from the N1E-115 cell line decreased from 4.4 ± 0.4 pA at 20°C to 2.6 ± 0.2 pA at 37°C (P = 0.0001), and to 1.5 ± 0.1 pA at 43°C (n = 10; P < 0.0001 between 20°C and 43°C and P = 0.018 between 37°C and 43°C). Data are depicted as means ± SEM. *, P < 0.05; **, P < 0.01; and ***, P < 0.001 (one-way ANOVA with Tukey HSD).

constant τ at the voltage of peak current as illustrated in the inset of Fig. 5 B. τ of $Na_V1.9$ at 20°C was 31.0 ± 9.1 ms, n = 5, and speeded to 8.0 ± 1.2 ms, n = 7, at 30°C, which represents a 3.9-fold increase (P = 0.01; Fig. 5 A). $Na_V1.8$ exhibited much faster values; 2.5 ± 0.3 ms at 20°C and 0.9 ± 0.1 ms at 30°C (n = 5), which corresponds to a 2.8-fold increase (P = 0.01; Fig. 5 B and Table 1).

As a measure of the speeding of the activation kinetics, we quantified the time to peak for the Na_V-channel subtypes and found that changing temperature from 10°C to 20°C or 30°C in DRGs of $Na_V1.8^{-/-}$ with 500 nM TTX in the bath reduced the time to peak of the presumptive $Na_V1.9$ current from 40.7 ± 11.2 to 12.2 ± 1.9 ms and to 3.5 ± 0.5 ms, respectively (n = 8; measured at −20 mV; Fig. 6 A). Between 10°C and 20°C, this represented a 3.3-fold change (P = 0.0004), and between 20°C to 30°C the change was 3.5-fold (P > 0.05; Fig. 6 F). DRGs derived from $Na_V1.9^{-/-}$ with 500 nM TTX in the bath measured at 10°C, 20°C, and 30°C had

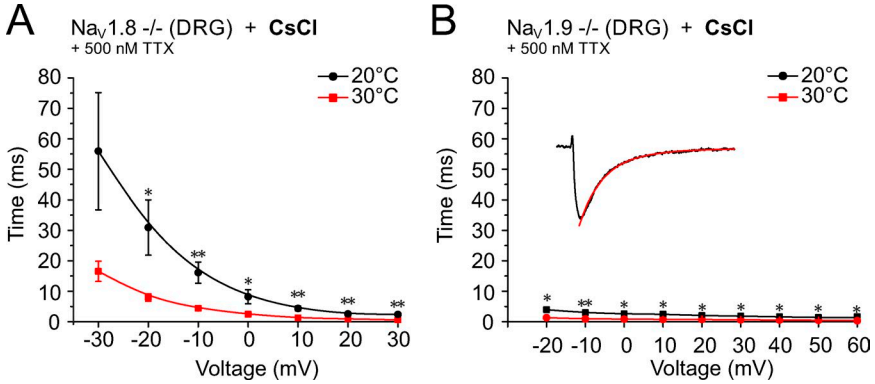

Figure 5. **Warming speeds the inactivation time constant τ of the TTXr sodium channels. (A and B)** The warming-induced increase in channel kinetics is illustrated by the reduction of the inactivation time constant, which decreased from 31.0 ± 9.1 ms at 20°C, n = 5, to 8.0 ± 1.2 ms at 30°C, n = 7 (P = 0.01) for $Na_V1.9$, measured at −20 mV (A) and from 2.5 ± 0.3 ms at 20°C to 0.9 ± 0.1 ms at 30°C, n = 5 (P = 0.01) for $Na_V1.8$, measured at 0 mV (B). This corresponded to decreases of 74% and 68%, respectively. Data are depicted as means ± SEM. *, P < 0.05; **, P < 0.01 (Student's t test).

Downloaded from http://rupress.org/jgp/article-pdf/150/8/1125/1798734/jgp_201711786.pdf by guest on 09 February 2026

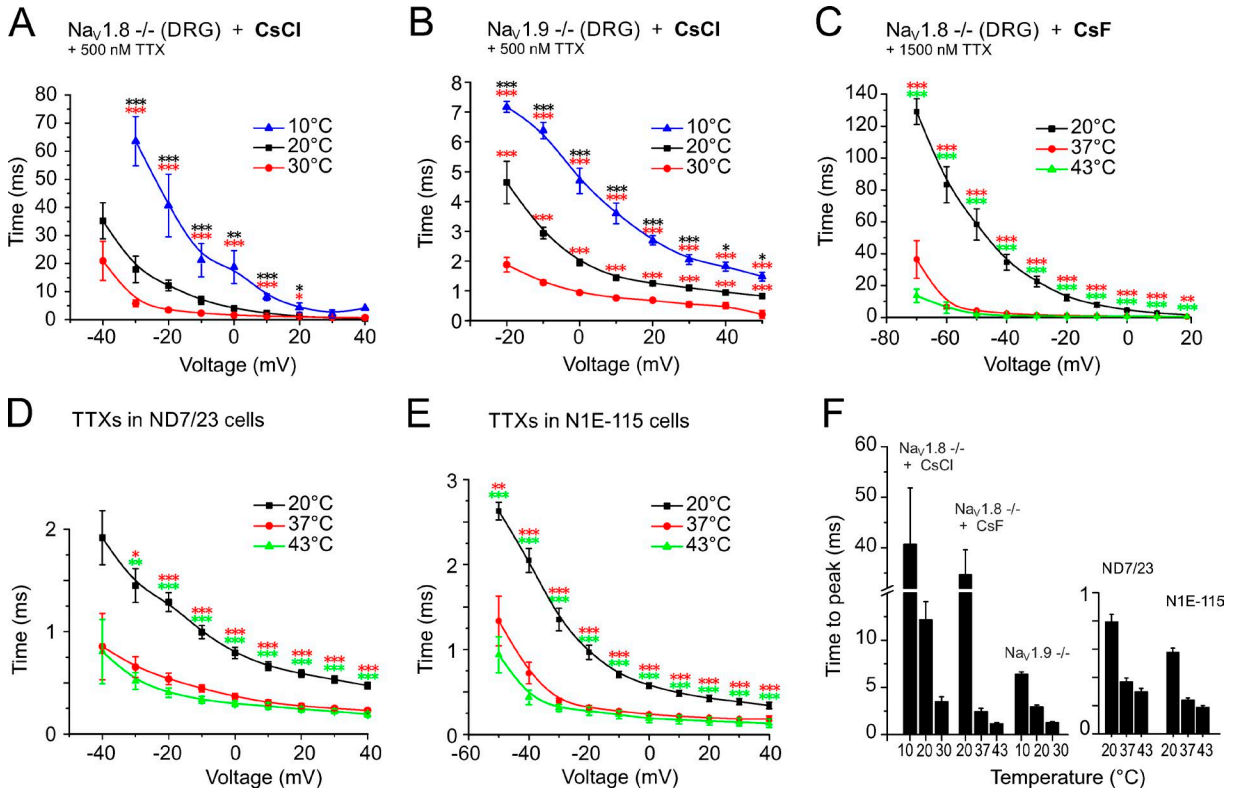

Figure 6. **Warming-induced speeding of the sodium channel activation kinetics quantified as time to peak.** Neurons were held at −90 mV and stimulated with 500-ms voltage pulses for DRGs and 100-ms pulses for TTXs currents from −90 mV up to +50 mV. The times to peak were calculated from the peak current amplitude at each voltage. **(A and B)** Recordings refer to Na$_V$1.8- and Na$_V$1.9-deficient cultured DRGs and were acquired at 10°C, 20°C, and 30°C using a CsCl-containing pipette solution in the presence of 500 nM TTX. **(C)** Recordings refer to Na$_V$1.8-deficient cultured DRGs and were acquired at 20°C, 37°C, and 43°C using a CsF-containing pipette solution in the presence of 1,500 nM TTX. **(D and E)** The TTXs current derived from ND7/23 and N1E-115 cell lines, respectively, were recorded with CsF in the pipette. **(F)** The largest change in time to peak was observed for the presumed Na$_V$1.9 current, which decreased 14.4-fold from 34.6 ± 5.0 ms at 20°C, n = 17, to 2.4 ± 0.3 ms at 37°C, n = 20, and 31.5-fold to 1.1 ± 0.1 ms at 43°C, n = 11. The changes in the TTXs currents were between 2.1- and 3.1-fold. Compare also Table 1 with Table 2. Data are depicted as means ± SEM. *, P < 0.05; **, P < 0.01; and ***, P < 0.001 (one-way ANOVA with Tukey HSD).

times to peak of 6.4 ± 0.3, 2.9 ± 0.2, and 1.3 ± 0.1 ms (n = 7, measured at −10 mV; Fig. 6 B), which corresponded to a speeding of the activation kinetic of 2.2-fold increases for both between 10°C and 20°C (P = 0.0008) and between 20°C and 30°C (P = 0.0003; Fig. 6 F and Table 1).

Remarkably, when testing higher temperatures of 37°C and 43°C with CsF-based intracellular solution, the times to peak for the presumptive Na$_V$1.9 current were further decreased: 2.4 ± 0.3 ms at 37°C (n = 20) and 1.1 ± 0.1 ms at 43°C (n = 11; Fig. 6 C) compared with 34.6 ± 5.0 ms at 20°C (n = 17). This corresponded to a speeding of 14.4-fold between 20°C and 37°C (P < 0.0001), and 31.5-fold between 20°C and 43°C (P < 0.0001; Fig. 6 F). In the ND7/23 cell line, the time to peak of the TTXs current was 0.58 ± 0.03 ms at 20°C (n = 24), 0.24 ± 0.02 ms at 37°C (n = 20), and 0.19 ± 0.01 ms at 43°C (n = 22; Fig. 6 D), which corresponded to a 2.4-fold change between 20°C and 37°C (P < 0.0001) and a 3.1-fold change between 20°C and 43°C (P = 0.0001; Fig. 6 F). In N1E-115 cells, the time to peak of the TTXs current was comparable: 0.79 ± 0.05 ms at 20°C, 0.37 ± 0.03 ms at 37°C, and 0.30 ± 0.03 ms at 43°C (n = 10, Fig. 6 E), and this corresponded to a speeding of 2.1-fold between 20°C and 37°C (P < 0.0001) and 2.6-fold between 20°C and 43°C (P < 0.0001; Fig. 6 F and Table 2).

Effects of increasing temperatures on membrane potential and input resistance

Because increasing temperature affects the cell parameters either specifically, through direct action on kinetics and channel gating, or nonspecifically, by reducing the quality of the seal and increasing the leak current, we first assessed nonspecific systematic effects of temperature on membrane voltage and input resistance. Our current clamp recordings at 20°C did not reveal any significant differences for the resting membrane potential between each group of DRGs derived from the different mouse strains. An increase in the temperature by 17°C from 20° to 37°C depolarized the mean resting membrane potential in all DRG recordings between 2 and 4 mV (Na$_V$1.8-deficient neurons in the presence of 500 µM TTX at 20°C/37°C: −56.3 ± 1.9/−53.3 ± 4.4 mV, n = 7, P = 0.29, paired t test; Na$_V$1.9-deficient neurons in the presence of 500 µM TTX at 20°C/37°C: −57.3 ± 2.7/−52.8 ± 2.2 mV, n = 11, P = 0.026, paired t test; Na$_V$1.8- and Na$_V$1.9-positive cells in the presence of 500 µM TTX at 20°C/37°C: −55.2 ± 2.0/−53.1 ± 1.7 mV, n = 13, P = 0.044, paired t test), but there were no significant differences between the groups (ANOVA followed by Tukey HSD post hoc test). After the 17°C increase in temperature, the input resistance appeared

Downloaded from http://rupress.org/jgp/article-pdf/150/8/1125/1798734/jgp_201711786.pdf by guest on 09 February 2026

reduced in all three groups of DRGs ($Na_V1.8$-deficient neurons in the presence of 500 µM TTX at 20°C/37°C: 760 ± 194/608 ± 128 MΩ, n = 17, P = 0.4, paired t test; $Na_V1.9$-deficient neurons in the presence of 500 µM TTX at 20°C/37°C: 536 ± 113/355 ± 45 MΩ, n = 14, P = 0.055, paired t test; $Na_V1.8$- and $Na_V1.9$-positive cells in the presence of 500 µM TTX at 20°C/37°C: 1151 ± 169/720 ± 107 MΩ, n = 12, P = 0.010, paired t test). The difference between the $Na_V1.9$-deficient DRGs and DRGs from the C57BL/6J background strain appeared significant for both temperatures (P = 0.039 at 20°C and 0.048 at 37°C, ANOVA, followed by Tukey HSD post hoc test).

In our measurements, we did not further differentiate between heat-sensitive and heat-insensitive DRG neurons, because heat-activated inward currents in cultured DRGs are exclusively caused by TRPV1 (Caterina et al., 2000; Zimmermann et al., 2005), whereas, according to behavioral experiments, heat transduction depends on the combination of three transducers, TRPA1, TRPM3, and TRPV1 (Vandewauw et al., 2018), and according to a large mRNA analysis, the expression of these three transducers is restricted to DRG subgroups that also express $Na_V1.9$ (Usoskin et al., 2015). To prevent a bias of the recordings caused by inconstant leak current, we manually clamped all cells at a virtual resting membrane potential of −80 mV, thereby keeping all Na_V channel isoforms in the resting state. With increasing temperature, the injected bias current was elevated accordingly. $Na_V1.8$-deficient neurons with 500 µM TTX at 20°C/37°C required −261 ± 81/−283 ± 85 pA, n = 18, P = 0.123, paired t test; $Na_V1.9$-deficient neurons with 500 µM TTX at 20°C/37°C were injected with −223 ± 88/−250 ± 65 pA, n = 9, P = 0.5, paired t test, and, $Na_V1.8$- and $Na_V1.9$-positive cells with 500 µM TTX at 20°C/37°C needed −101 ± 18/−148 ± 31 pA (n = 22, P = 0.004, paired t test). No significant differences between the injected currents were apparent for the different groups of DRGs for both temperatures (ANOVA, followed by Tukey HSD post hoc test).

This analysis ruled out large nonspecific effects of temperature on the membrane parameters. Therefore, the observed effect of temperature on the $Na_V1.9$ peak current, conductance, and integrated peak area imply a larger contribution of the $Na_V1.9$ current to the action potential current at higher temperatures than previously recognized. To study this effect, we measured action potentials in current clamp mode in both $Na_V1.8$- and $Na_V1.9$-deficient DRG neurons.

Nociceptor action potentials at rising temperatures need $Na_V1.9$ to reach the threshold

As previously outlined, we analyzed the temperature dependence of action potential generation in DRG neurons derived from $Na_V1.8$- and $Na_V1.9$-deficient mice in the presence of TTX, and on the combined $Na_V1.8$ and $Na_V1.9$ currents of WT neurons (derived from the C57BL/6J background strain) in the presence of TTX (TTXr WT; Fig. 7). The action potential threshold was measured as the inflection point of the action potential rising phase, as illustrated in Fig. 7 C. The lack of $Na_V1.9$ resulted in a depolarization of the voltage threshold of activation by more than 17 mV at 20°C from −32.3 ± 2.4 mV measured in TTXr WT, n = 20, to −14.6 ± 2.8 mV, n = 15 (P = 0.0002; Fig. 7, A and B). An increase in the temperature to 37°C further depolarized the threshold in $Na_V1.9$-deficient neurons by 18 mV to +3.3 ± 4.9 mV, n = 8 (P < 0.0001; Fig. 7, A and B). In contrast, 37°C depolarized the TTXr WT neurons only by 5 mV to −26.6 ± 2.4 mV, n = 23. Similarly, the $Na_V1.8$-deficient action potentials demonstrated almost no change of the threshold at 20°C (−26.8 ± 3.9 mV, n = 12) or 37°C (−29.1 ± 3.3 mV, n = 16; Fig. 7, A and B).

Evidently, $Na_V1.9$ has a huge influence on the action potential threshold, and its lack becomes even more apparent when the temperature rises. Our results indicate that $Na_V1.9$ is required in a large population of neurons, presumably in all neurons that are dedicated to heat transduction and express TRPA1, TRPM3, and TRPV1 (Usoskin et al., 2015; Vandewauw et al., 2018), to reach the depolarized threshold of the $Na_V1.8$-mediated action potentials. Also, with regard to the increased activation kinetics (quantified as time to peak) and decreased inactivation time constants, this finding raises the question of whether $Na_V1.9$ serves primarily as an amplifier of heat-activated membrane depolarization or whether $Na_V1.9$ can act as an independent generator of action potentials.

Rising temperatures boost $Na_V1.9$-dependent action potentials

In $Na_V1.8$-deficient neurons, in the presence of TTX in the bath, we were able to record action potentials with a clear inflection point and an overshoot reaching beyond 0 mV. At 20°C, the overshoot reached 10.9 ± 2.5 mV, n = 13, and at 37°C, it reached 15.3 ± 2.4 mV, n = 17 (Fig. 7 D). The overshoot was visibly smaller, at any temperature, than in neurons with $Na_V1.8$-dependent action potentials (Fig. 7 E), where the overshoot measured 52.8 ± 4.3 mV at 20°C and 57.0 ± 1.8 mV at 37°C (n = 11), but warming the same $Na_V1.8$-deficient neurons to 37°C strikingly speeded the action potential kinetics at constant voltage threshold, much in contrast to the $Na_V1.8$-mediated action potential (Fig. 7, D and E). Therefore, we further evaluated the characteristics of $Na_V1.8$- and $Na_V1.9$-mediated action potentials at 37°C. The most remarkable observation in the $Na_V1.9$-mediated action potential at 37°C, compared with 20°C and $Na_V1.8$, is the massive speeding of the upstroke. At 37°C, the slope of the $Na_V1.9$-mediated action potential was accelerated 5.8-fold, n = 17, whereas $Na_V1.8$-mediated action potentials became only 2.3-fold faster, n = 5 (P = 0.013 compared with $Na_V1.9$-mediated action potentials) and action potentials with both current components, $Na_V1.8$ and $Na_V1.9$, became 2.5-fold faster, n = 21 (P = 0.0002 compared with $Na_V1.9$-mediated action potentials; Fig. 7 F). Action potentials with both current components were not significantly different from action potentials derived from $Na_V1.9^{-/-}$ neurons.

An essential feature of nociceptors is their ability to generate repetitive action potential firing. We analyzed the capability of each TTX-resistant sodium channel subtype to generate a series of action potentials in response to a depolarizing stimulus at both 20°C and 37°C using the double rheobase current (Fig. 8). At 37°C, the presence of $Na_V1.9$ alone allowed repetitive firing in 10 of 17 neurons, and a mean of 8.2 ± 2.1 action potentials were generated per 200-ms current pulse (Fig. 8, A and B), whereas, at 20°C, only 3 of 17 neurons produced repetitive firing in response to the same stimulus (2.3 ± 0.9 action potentials). The findings were

Downloaded from http://rupress.org/jgp/article-pdf/150/8/1125/1798734/jgp_201711786.pdf by guest on 09 February 2026

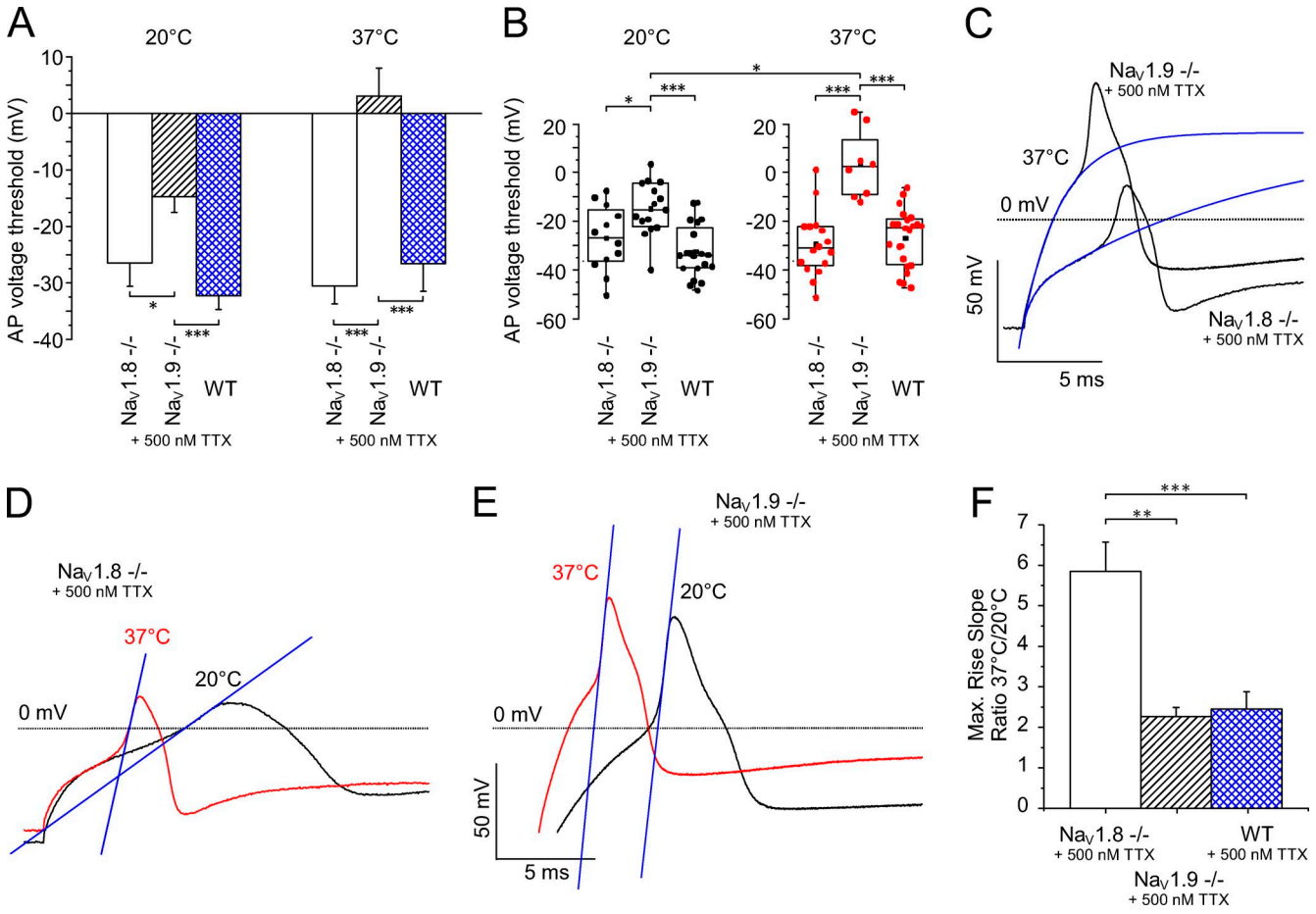

Figure 7. **TTXr sodium channel subtype $Na_V1.9$ generates action potentials at 37°C and becomes essential for reaching the action potential threshold when the temperature rises. (A)** Contribution of sodium channel subtypes $Na_V1.9$ and $Na_V1.8$ to the action potential threshold at 20°C (left columns) and 37°C (right columns). All measurements were performed in the presence of 500 nM TTX in the bath solution in DRGs derived from C57BL/6J or $Na_V1.9$- or $Na_V1.8$-deficient mice. At 20°C and 37°C, the action potential threshold of the combined $Na_V1.8$ and $Na_V1.9$ current was −32.3 ± 2.4 mV, n = 20, and 26.6 ± 2.4 mV, n = 23, respectively. In the absence of either $Na_V1.8$ or $Na_V1.9$, the action potential thresholds at 20°C were depolarized to −26.8 ± 3.9 mV, n = 12, and −14.6 ± 2.8 mV, n = 15, respectively. At 37°C, lack of $Na_V1.9$ depolarized the threshold of the $Na_V1.8$-dependent action potentials to +3.3 ± 4.9 mV, n = 8. **(B)** Distribution and statistical analysis of the threshold values of individual measurements are displayed in A. **(C)** Typical action potentials from $Na_V1.8^{-/-}$ and $Na_V1.9^{-/-}$ DRG neurons at 37°C in the presence of 500 µm TTX with extrapolation of the threshold, as indicated by the blue curves. **(D–F)** Typical action potentials from $Na_V1.8^{-/-}$ and $Na_V1.9^{-/-}$ DRGs at 20°C and 37°C with extrapolation of the rise slope (superimposed blue lines) to illustrate the effect of warming. The speeding of the upstroke was largest (D) for the putative $Na_V1.9$-mediated action potentials ($Na_V1.8^{-/-}$ with 500 nM TTX, n = 17) and reached 5.8-fold, whereas it was only 2.3-fold (E) for the $Na_V1.8$-mediated action potentials ($Na_V1.9^{-/-}$ with 500 nM TTX, n = 5) and 2.5-fold (F) for action potentials generated by a combination of $Na_V1.8$ and $Na_V1.9$ (n = 21). Data are depicted as means ± SEM. *, P < 0.05; **, P < 0.01; and ***, P < 0.001 (one-way ANOVA with Tukey HSD).

not significantly different for TTXr WT neurons, few of which exhibited repetitive firing, with a mean rate of 5.3 ± 1.3 action potentials (4 of 11 neurons) at 20°C. This number increased at 37°C to 7.2 ± 1.4 action potentials in 6 of 11 investigated cells. Most remarkably, the presence of $Na_V1.8$ alone was insufficient to initiate repetitive firing at both temperatures in any of the tested neurons (Fig. 8, A and C; n = 15).

Our voltage-clamp experiments demonstrated that warming causes an impressive gain of function of $Na_V1.9$, and our current-clamp experiments indicate that, with rising temperatures, $Na_V1.9$ becomes the key molecule, bringing the neuron reliably to firing threshold and contributing in large part to the upstroke of the action potential. Our next aim was to isolate the exact contribution of TTXs and the two TTXr Na_V channel isoforms to the generation of heat-resistant action potential in native skin nociceptors.

Two lines of heat-sensitive nociceptors in the skin require TTXr sodium channels

The isolated skin-nerve preparation allows the focal application of heat and TTX to a cutaneous receptive field of a single intact nociceptor and permits recording of the propagated action potentials. Using 1 µM TTX applied directly to the nociceptor terminals, we identified two populations of heat responses with distinct features. The first population occurred frequently, and its heat response was inhibited by TTX; thus a TTXs sodium channel subtype contributed to the electrogenesis at raised temperatures (Fig. 9 B). In the presence of TTX, the fibers lost electrical excitability around skin temperature but remained excitable when the receptive field was cooled, which implies that $Na_V1.8$ is expressed as well (Zimmermann et al., 2007). This fiber type produced action potential counts during a 20-s ramp rising from 30°C to 50°C of 15.4 ± 8.1, n = 16 (Fig. 9, B, D, and E), and its

Downloaded from http://rupress.org/jgp/article-pdf/150/8/1125/1798734/jgp_201711786.pdf by guest on 09 February 2026

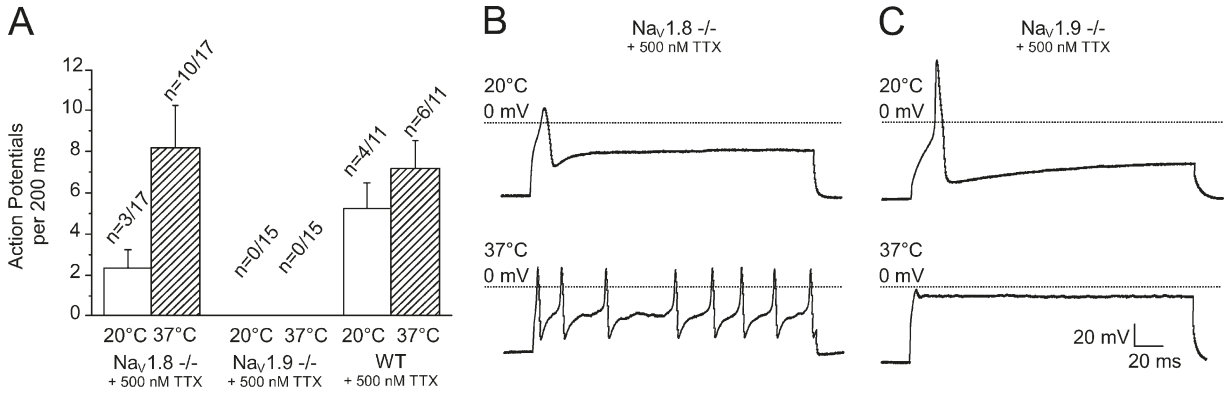

Figure 8. **TTXr sodium channel subtype Na$_V$1.9 enables repetitive firing in nociceptors when the temperature rises.** DRGs derived from the C57BL/6J background strain (WT) or Na$_V$1.9- or Na$_V$1.8-deficient mice were subjected to a 200-ms depolarizing current pulse at 20°C and 37°C. **(A)** Action potential frequency at 37°C compared with 20°C (the first evoked action potential was not counted). **(B and C)** Representative recordings from Na$_V$1.8$^{-/-}$ (B) and Na$_V$1.9$^{-/-}$ (C) DRGs illustrate that the presence of Na$_V$1.9, but not Na$_V$1.8, enables repetitive firing at increased temperatures. Data are depicted as means ± SEM. *, P < 0.05; **, P < 0.01; and ***, P < 0.001 (one-way ANOVA with Tukey HSD).

response was characterized by a low mean firing frequency (1.7 ± 0.9/s, *n* = 16; Fig. 9 E), a peak firing frequency less than 10/s (4.5 ± 4.0/s, *n* = 16; Fig. 9 E), and thresholds ranking near the human heat pain threshold (39.9 ± 3.4°C, *n* = 16; Fig. 9 F). The second polymodal nociceptor type was less frequent, and it produced large responses to the same ramp-shaped heat stimulus of 121.8 ± 24.3 action potentials in 20 s, *n* = 6 (Fig. 9, A, D, and E). The heat response appeared only slightly reduced when the receptive field was exposed to TTX, indicating that TTXr sodium channel subtypes initiated the electrogenesis (compare Fig. 11 A). The responses were characterized by high mean firing (21.6 ± 7.9/s, *n* = 6) and high peak firing rates (47.8 ± 8.4/s, *n* = 6; Fig. 9 E), and their thresholds were lower (34.6 ± 2.3°C, *n* = 6; Fig. 9 F). According to their features, we named the TTX-blocked nociceptor type with the small response S-type C-mechanoheat (CMH) and the TTX-insensitive nociceptor type with the large response L-type CMH (Fig. 9, A–F). The slope of the stimulus response function for both fiber types is comparable, but the response shifted in L-type CMH to 10-fold higher firing rates at all temperatures (Fig. 9 C and Table 3).

These findings characterized the properties of the polymodal nociceptors in response to rapid rises in temperature (1°C/s). We next investigated how heating affects the action potential threshold in the nociceptors by measuring the excitability threshold, while simultaneously raising temperature at a rate of 0.1°C/s from 30°C to 50°C. We programmed a feedback-controlled algorithm that regulates the current intensity applied to the receptive nerve terminal and tracked the threshold at a rate of 1 impulse/s (for details, see Materials and methods). We found that all S-type CMH fibers maintained constant excitability up to the maximum ramp temperature of 50°C, *n* = 7 (L-type CMH cannot be tracked because of their vigorous response during heat ramps; Fig. 10, A and C). We compared this finding to the Na$_V$1.8- and TRPM8-positive C-mechanocold (CMC) fibers (Zimmermann et al., 2011; Vetter et al., 2013; Winter et al., 2017), because they lack heat transducer channels and, in case of TRPM8 expression, have no or low Na$_V$1.9 (Lolignier et al., 2015). In contrast to the CMH fibers, excitability in CMC fibers (*n* = 12) always decreased above 40°C and was lost, on average, at 45.8 ± 2°C with the current intensity reaching the maximum stimulation intensity of 10 mA, *n* = 7 (Fig. 10, B and C). Remarkably, in 66% of the tracked CMH fibers, the threshold decreased above 40°C, which was followed by heat-induced firing, which transiently hindered the tracking of the threshold. This effect is caused by the activation of heat transducer channels (TRPA1, TRPM3, TRPV1; gray inset in Fig. 10 A). When 1 µM TTX was applied at 30°C and the receptive field heated, both S-type CMH (*n* = 7) and CMC (*n* = 5) fibers lost excitability at similar temperatures of ∼34°C, but they regained excitability when the receptive field was cooled to <28°C; as we previously described, this occurs by virtue of Na$_V$1.8 and the cold-induced increase in membrane resistance (Zimmermann et al., 2007). To recognize the individual contributions of Na$_V$1.8 and Na$_V$1.9 to electrogenesis in both CMH types, we next quantified the encoding deficits of the two types of CMH responses in skin-nerve preparations of Na$_V$1.8- and Na$_V$1.9-deficient mice.

The signature Na$_V$ channel of L-type CMHs is Na$_V$1.8, and Na$_V$1.9 dominates in S-type CMHs

In Na$_V$1.8-deficient skins, CMHs appear at a frequency similar to the underlying C57BL/6J strain of 50–70% (Zimmermann et al., 2005, 2009), and we characterized 20 heat-responsive C-fibers. In Na$_V$1.9$^{-/-}$, C-fibers had high mechanical thresholds; we applied high pressure with a blunt glass rod as mechanical search stimulus and located 10 CMHs, all with L-type–like response, in a population of 35 fibers (Fig. 11 B). In both knockout lines, distinction between L-type and S-type CMH was made according to the peak firing rate difference identified in the underlying WT strain. We used >10/s as threshold to assign L-type, as implied by Fig. 9 E. Intriguingly, nine Na$_V$1.9-deficient CMHs were clearly L-type, and the one remaining showed irregular burst-like activity and could not be allocated to any of the types (Fig. 11, B and E); in 35 fibers, Na$_V$1.9-deficient nociceptors never showed the otherwise frequent S-type–like heat response (Fig. 11 E). In Na$_V$1.8$^{-/-}$, six CMHs had peak firing rates >10 and were classified as L-type (Fig. 11, B and E). These fibers also had larger heat responses than the remaining 14 CMHs, which were assigned S-type (Table 3 and

Downloaded from http://rupress.org/jgp/article-pdf/150/8/1125/1798734/jgp_201711786.pdf by guest on 09 February 2026

Table 3. **Properties of S- and L-type CMH fibers**

Fiber type	*n*	Response magnitude	Peak discharge	Mean discharge	Threshold temperature	Maximum encoded T
					°C	
C57BL/6J L-type	6	121.8 ± 24.3	47.8 ± 8.4	21.6 ± 7.9	34.6 ± 2.3	50.8 ± 1.0
C57BL/6J L-type, after TTX	4	79.0 ± 27.9	39.1 ± 11.9	15.3 ± 7.1	35.7 ± 2.8	50.6 ± 2.3
$Na_V1.9^{-/-}$, L-type	9	76.7 ± 33.6	66.1 ± 27.4	29.5 ± 15.0	38.1 ± 6.1	45.2 ± 4.3
$Na_V1.8^{-/-}$, L-type	6	50.2 ± 36.0	24.5 ± 12.3	9.2 ± 4.1	37.4 ± 5.6	50.1 ± 2.4
C57BL/6J S-type	16	15.4 ± 8.1	4.5 ± 4.0	1.7 ± 0.9	39.9 ± 3.4	49.8 ± 1.1
$Na_V1.8^{-/-}$, S-type	14	11.5 ± 6.6	4.5 ± 3.3	2.1 ± 1.6	41.2 ± 4.2	49.8 ± 1.8

Data are mean ± SD.

Fig. 11, E and F). The allocation to the two groups made encoding deficits apparent for both groups in both transgenic genotypes. The $Na_V1.9$-deficient L-type responses had a reduced dynamic range and, in most of the fibers ($n = 6$), the number of heat-activated action potentials was reduced at higher temperature (Fig. 11, B, D, and E; and Tables 3 and 4). The stimulus-response function was steeper and shifted to lower temperatures by ∼4°C (Fig. 11 C, compare Fig. 9 C), possibly because of adaptation mechanisms in transgenic mice, as previously observed for the $Na_V1.8$-deficient strain (Matsutomi et al., 2006). The responses were partially or not blocked by application of TTX to the receptive field and presumably generated by $Na_V1.8$ in combination with a TTXs Na_V channel (Fig. 11 D). In contrast to $Na_V1.9$-deficient preparations, in $Na_V1.8$-deficient mice, no L-type CMH was able to build action

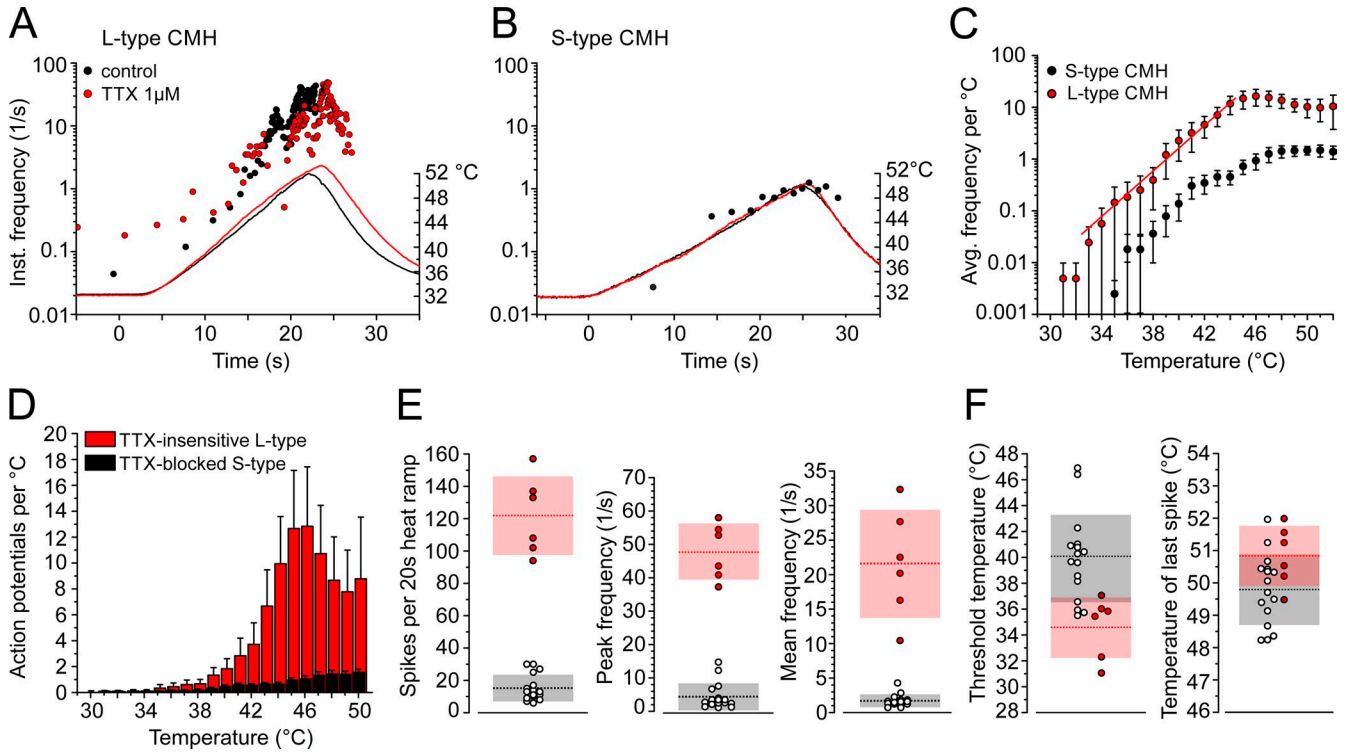

Figure 9. **Characteristics of two distinct types of polymodal nociceptors, TTX-insensitive L-type and TTX-blocked (S-type). (A and B)** Representative recording of two heat-sensitive polymodal nociceptors, TTX-insensitive (A) and TTX-blocked (B), as found in mouse saphenous-nerve skin preparations. Instantaneous discharge rates in response to heating of the receptive field are shown. Circles represent action potentials. Action potentials discharged after treatment with TTX 1 µM are shown as red closed circles (A). Heat stimuli were ramp-shaped and are plotted as temperature time course. **(C)** Stimulus response diagrams for TTX-insensitive (red, $n = 6$) and TTX-blocked (black, $n = 16$) heat responses (from three-point averaged data). **(D)** Averaged histogram of heat responses of TTX-insensitive (red, $n = 6$) and TTX-blocked (black, $n = 16$) heat responses. **(E)** TTX-insensitive heat responses share larger response magnitudes ($P = 0.0004$) and higher peak and mean discharge rates (both $P = 0.0004$). **(F)** Dynamic range of CMH fibers; L-type CMH receptors have lower temperature thresholds ($P = 0.02$) but comparable dynamic range ($P = 0.7$). Light gray and red blocks are SD; dotted lines represent the mean of TTX-insensitive (red) and TTX-blocked (black) values. Data are depicted as means ± SEM. All P values refer to the Mann–Whitney *U* test.

Downloaded from http://rupress.org/jgp/article-pdf/150/8/1125/1798734/jgp_201711786.pdf by guest on 09 February 2026

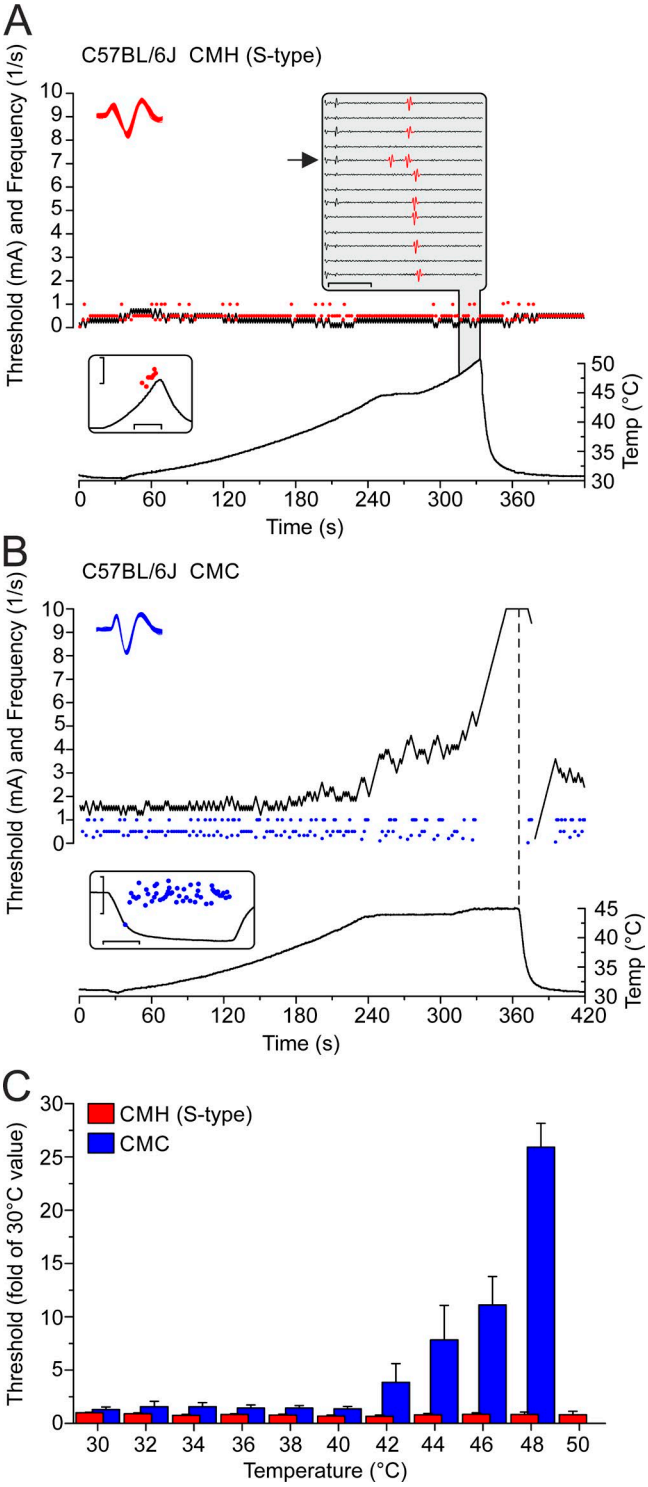

Figure 10. **CMH, but not CMC, nociceptors remain excitable above 45°C.** To test the temperature dependence of excitability, threshold tracking of polymodal nociceptors was performed based on current injections into the receptive field at slowly increasing temperatures (0.1°C/s). Evoked action potentials operated a feedback-controlled tracking algorithm that served to adjust the current intensity in steps of ± 0.1 mA at a rate of 1/s. Depending on the individual fiber, the stimulus length was set between 0.5 and 2 ms. **(A)** Representative recording of one S-type C57BL/6J CMH fiber. The nociceptor's electrical excitability remains unchanged when the temperature increases to 50°C. Red circles are electrically evoked action potentials; the black line signifies the electrical threshold, and the bottom graph shows the temperature time course at the receptive field where the electrode is placed. The top left inset provides a collapsed view of the shapes of all electrically evoked action potentials depicted in the main graph as red circles. The bottom left inset shows that the CMH's heat response to a 20-s ramp from 30° to 50°C is typical for S-type CMHs; the scales are the instantaneous frequency on a log scale (1 – 10/s; y) and the time (10 s; x). The top right inset (gray) provides a waterfall view of a series of consecutive 150-ms traces of the electrically evoked action potentials marked in red (increasing temperatures from top to bottom, ∼48°–50°C) with the axes signifying the voltage (scale ±10 V; y) and the time (scale 50 ms; x). Arrows mark the heat-activated action potentials, which interfere with threshold tracking (leading to slowing of the latency in subsequent traces). **(B)** In contrast to CMHs, in TRPM8-positive cold nociceptors (CMC), electrical excitability reduces with heating, and, above ∼45°C, CMCs become reversibly unresponsive. The vertical dashed bar follows the temperature ramp's peak. Blue circles are electrically evoked action potentials, the black line represents the electrical excitation threshold, and the bottom graph indicates the temperature time course at the receptive field where the electrode is placed. The top inset provides a collapsed view of the action potential shapes of all electrically evoked action potentials depicted in the main graph as individual blue circles, and the bottom inset shows that the CMC has a signature cold response of a TRPM8-expressing cold nociceptor, where the axes represent the instantaneous frequency on a log scale (scale 0.1–10/s; y), and the time (scale 20 s; x). **(C)** Histogram of threshold–temperature relationships comparing CMC fibers (n = 7) and S-type CMH fibers (n = 12) from C57BL/6J mice. The electrical threshold is expressed as the fold change of the mean basal threshold value determined during at least 60-s tracking at 30°C. At 50°C, the CMC threshold exceeded the maximum of 10 mA of the current stimulator. Data are depicted as means ± SEM.

potentials in the presence of TTX. We conclude that $Na_V1.9$, albeit with its kinetics greatly speeded up, is incapable of discharging independent, propagated action potentials in terminals during heating in the absence of any of the other two Na_V channels, $Na_V1.8$ and presumably $Na_V1.7$; this appears to be in contrast to the isolated cultured somata (Figs. 7 and 8). $Na_V1.8^{-/-}$ L-type CMHs had an unchanged dynamic range, but the response magnitude as well as the firing rate appeared reduced, with the slope of the stimulus-response function flattened (Fig. 11, B, C, and E). Absence of $Na_V1.8$ did not affect the heat-encoding properties of S-type CMHs in terms of the magnitude of the response, peak discharge, and dynamic range; although the effect was insignificant, they appeared to have reduced averaged responses at the peak ramp temperature as estimated from the histogram (Tables 1 and 2 and Fig. 11 F). Remarkably, this encoding deficit became evident and measurable in the threshold tracking experiments (see below and Fig. 12 C).

The lack of S-type responses in $Na_V1.9^{-/-}$ was apparent and appeared puzzling given the high occurrence of this fiber type in the underlying C57BL/6J strain. We also identified CMC fibers (37%; n = 13) and thermo-insensitive units (34%; n = 12). The cold-sensitive fibers all had cold responses comparable to TRPM8-expressing CMC-fibers (Zimmermann et al., 2011; Vetter et al., 2013; Winter et al., 2017). Applying the tracking protocol, we found that $Na_V1.9$-deficient CMCs ceased to be excitable at 43.3 ± 2.4°C, insignificantly lower than the C57BL/6J CMC fibers (n = 9; not depicted). Concerning the thermo-insensitive units, we found that they maintained excitability up to 50°C with an almost unchanged threshold and, like the S-type CMH in the underlying C57BL/6J strain, they discharged irregularly during the slow heat ramp (observed in 57% of the fibers). From these

Downloaded from http://rupress.org/jgp/article-pdf/150/8/1125/1798734/jgp_201711786.pdf by guest on 09 February 2026

Table 4. **Percent contribution of TTXs, $Na_V1.8$, and $Na_V1.9$ to L-type CMH heat response changes with temperature (referring to insets in Fig. 11, A and B)**

Na_V channel	Temperature (±3°C)				
	38°C	41°C	44°C	47°C	50°C
TTXs (C57BL/6J)	36.8	33.3	31.2	8.7	1.8
TTXr (C57BL/6J)	63.2	66.6	68.8	91.3	98.2
NaV1.8 + TTXs (NaV1.9−/−)	73.2	85.5	70.0	39.7	32.8
NaV1.9 + TTXs (NaV1.8−/−)	26.8	14.5	30.0	60.3	67.2

findings, we concluded that lack of $Na_V1.9$ affects the capacity of S-type CMH fibers to fire in response to steeply rising heat (~1°C/s), but not slowly rising heat (~0.1°C/s). The tracking protocol identified these fibers without ambiguity as incapacitated S-type CMHs (Fig. 12, A and C). Therefore, keeping the encoding deficit in response to fast-rising heat in mind (Fig. 11 E), the overall occurrence of CMHs is not different from the C57BL/6J background strain. In contrast to lack of $Na_V1.9$, lack of $Na_V1.8$ had a distinct effect on threshold excitability at noxious high temperatures: in all CMH fibers—without any exception—the excitability decreased and or was reversibly lost at 47.3 ± 1.8°C (Fig. 12, B and C).

From these experiments, we conclude that $Na_V1.9$ is the signature Na_V subtype in S-type CMH fibers and is required to secure responses to fast (1°C/s), but not slow (0.1°C/s), temperature rises, whereas $Na_V1.8$ gains function above 46°C and ultimately encodes the heat-resistant action potential.

$Na_V1.8$ and $Na_V1.9$ label two independent lines of polymodal nociceptors

We finally assessed the contribution of each isolated TTXr sodium channel in behavioral experiments using the Hargreave's assay, where an infrared heat beam is directed on the hindpaw of the mouse, and the reaction time to withdraw from noxious heat is measured (Fig. 13). WT mice withdrew after 9.0 ± 0.7 s

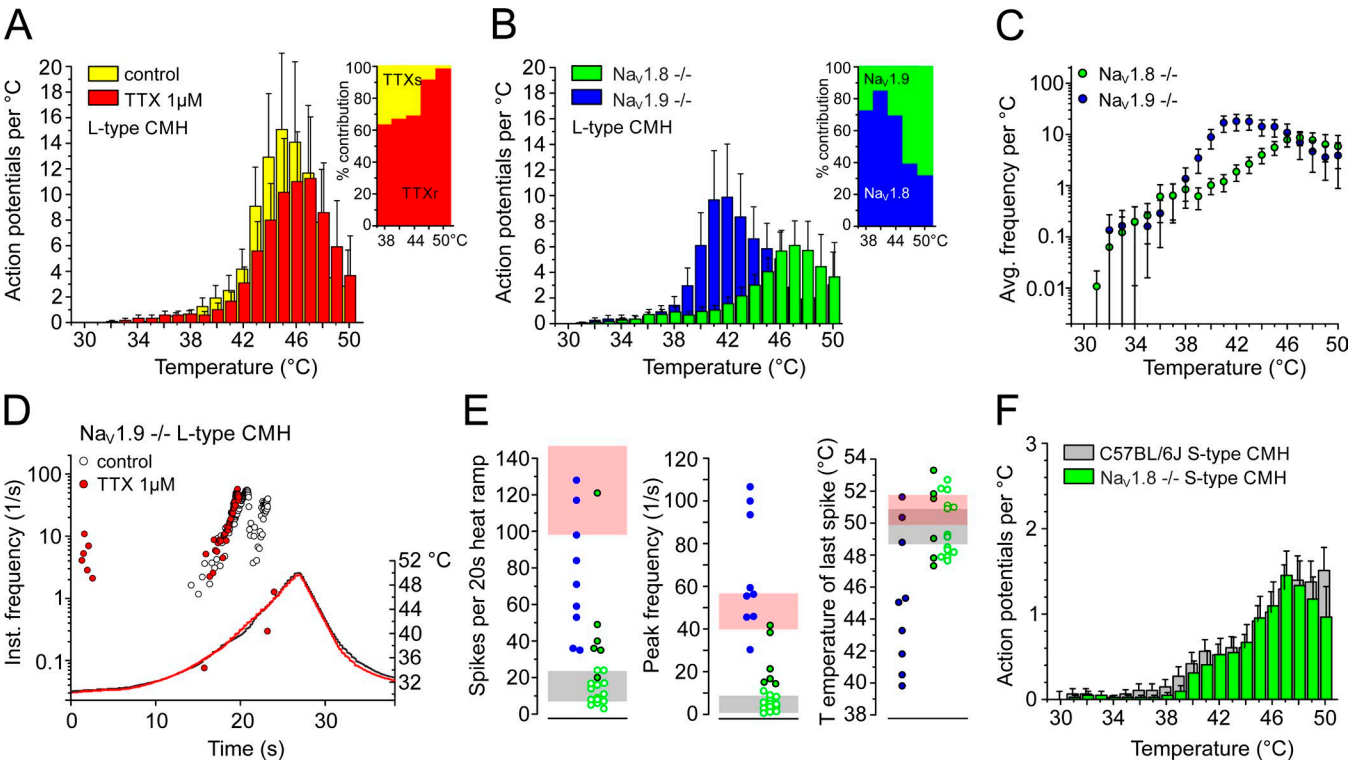

Figure 11. **Heat encoding deficits in $Na_V1.8$- and $Na_V1.9$-deficient S- and L-type CMHs. (A)** Averaged histogram of heat responses of C57BL/6J L-type CMH before (yellow) and in the presence of TTX 1 µM (red; n = 4). Inset: Proportion of the TTX-blocked heat response calculated for the respective temperature ranges. TTXs and TTXr indicate the proportion of action potentials mediated by TTXs and TTXr Na_V channel subtypes, respectively (compare Table 3). **(B)** Histogram of L-type CMH heat responses of $Na_V1.8$-deficient (n = 6) and $Na_V1.9$-deficient fibers (n = 9) illustrate encoding deficits compared with the responses from C57BL/6J shown in A and Fig. 9. Inset: Estimated proportion contributed by $Na_V1.9$ (green) and $Na_V1.8$ (blue) at the respective temperature ranges. Note that both components contain the TTXs component (compare Table 3). **(C)** Stimulus response diagrams of mean discharge rate and temperature for $Na_V1.9^{-/-}$ (n = 9) and $Na_V1.8^{-/-}$ (n = 6) heat responses (from three-point averaged data). $Na_V1.9^{-/-}$ L-type CMHs achieve a higher slope at lower temperatures compared with WT and $Na_V1.8^{-/-}$. **(D)** Original recording from a $Na_V1.9$-deficient L-type CMH heat response before (white circles) and in the presence of TTX 1 µM (red). Each circle represents an action potential in response to heating. **(E)** $Na_V1.9$-deficient CMHs respond to fast rising heat-ramps (1°C/s), with peak discharge rates comparable to the L-type CMHs but reduced response magnitude and dynamic range (blue circles). $Na_V1.8$-deficient heat responses of L-type CMH (closed green circles), but not S-type CMH (open green circles), are smaller and exhibit lower peak discharge rates in contrast to the C57BL/6J background strain, but have unchanged dynamic range. Light gray and light red blocks represent the SD of the respective C57BL/6J values of S-type and L-type CMHs illustrated in Fig. 9 (E and F). **(F)** Averaged histogram of $Na_V1.8$-deficient S-type CMH responses (green) in comparison to C57BL/6J S-type CMHs (gray, taken from Fig. 9 D). Data are depicted as means ± SEM.

Downloaded from http://rupress.org/jgp/article-pdf/150/8/1125/1798734/jgp_201711786.pdf by guest on 09 February 2026

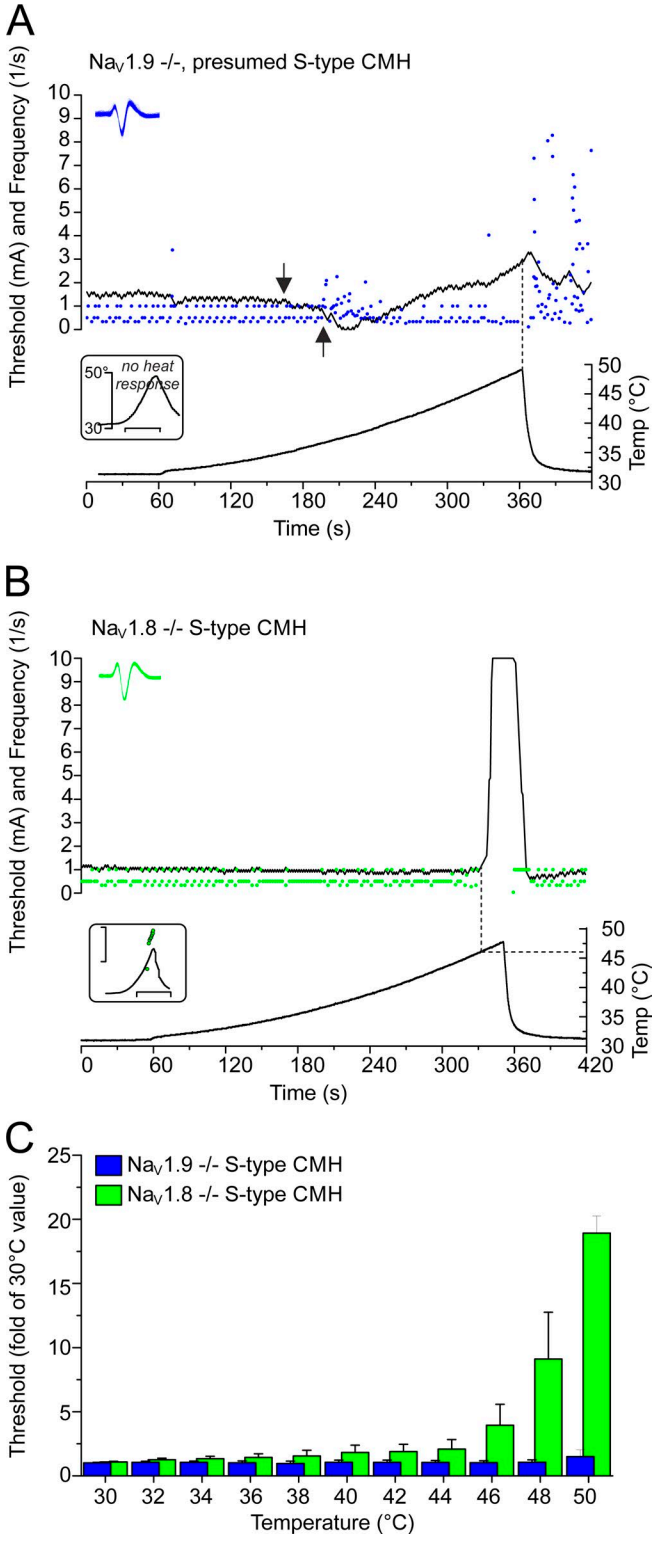

Figure 12. **Threshold tracking of Na$_V$1.8- and Na$_V$1.9-deficient S-type CMHs reveals Na$_V$1.8 to be essential for electrogenesis >46°C and Na$_V$1.9 to be essential for electrogenesis during fast, but not slowly, rising heat.** **(A)** Lack of Na$_V$1.9$^{-/-}$ does not impair electrogenesis during slowly rising heat (0.1°C/s), and excitability remains relatively constant up to 50°C. The arrows point at the typical decrease in threshold caused by the heat transduction channel activation, which precedes the discharge of heat-induced action potentials. The blue circles are action potentials evoked by electrical stimulation and heating, the black line represents the electrical threshold, and the temperature time course is shown at the bottom. Lack of Na$_V$1.9$^{-/-}$ results in lack of action potential discharge in response to fast ramp-shaped heating (1°C/s) of S-type CMHs as illustrated for this fiber in the bottom inset (no action potentials; x-axis scale, 10 s). The top inset provides a collapsed view of the action potential shapes of all electrically and heat-evoked action potentials (blue circles in main graph). **(B)** In Na$_V$1.8$^{-/-}$ S-type CMHs, the excitability is abruptly lost a few degrees before the temperature reaches 50°C. The bottom inset shows that the CMH has the typical heat response of S-type CMHs, where the axes represent the instantaneous frequency on a log scale (scale 1–10/s; y), and the time (scale 20 s; x). Each green circle represents one action potential evoked by electrical stimulation, the black line visualizes the electrical threshold, and the bottom graph depicts the temperature time course at the receptive field. The top inset provides a collapsed view of the action potential shapes of all electrically evoked action potentials (green circles in main graph). **(C)** Histogram of threshold–temperature relationships for Na$_V$1.9$^{-/-}$ (n = 7; blue bars) and Na$_V$1.8$^{-/-}$ (n = 5; green bars). The electrical threshold is expressed as fold of the mean basal threshold value determined during at least 60-s tracking at 30°C, before the rising heat. Data are depicted as means ± SEM.

(Fig. 13 B). We reproduced previous experiments demonstrating mild deficits in heat pain sensing for both Na$_V$1.8- (Akopian et al., 1999) and Na$_V$1.9-deficient mice (Minett et al., 2014). To remove the contribution of the TTXs subtypes, we injected 3 µM TTX in a volume of 20 µl intracutaneously in the paw under light sevoflurane anesthesia (shortest decay rate of all inhalation anesthetics). The heat withdrawal latencies subsequently increased for Na$_V$1.8$^{-/-}$ from 12.1 ± 1.1 to 16.3 ± 1.5 s ($P < 0.001$) and, for Na$_V$1.9$^{-/-}$, from 12.5 ± 1.5 to 15.1 ± 1.7 s ($P < 0.001$) compared with animals of the C57BL/6J background strain that had an unchanged withdrawal latency at 7.6 ± 0.7 s in the presence of TTX (n = 8 for all groups; Fig. 13 A). This experiment illustrates the importance of the TTXs sodium channel subtypes for the activation of heat-sensitive nociceptors at an individual's heat pain threshold, as long as either Na$_V$1.8 or Na$_V$1.9 is also present.

Discussion

Temperature is a significant physiological stressor and driver of adaptive evolution. Although invertebrates possess only two sodium channel subtypes, adaptive sequence evolution has produced 10 unique sodium channel subtypes in mammals and favored adaptation to sophisticated neuronal functions (Zakon, 2012). This includes, for example, the evolution of communication signals in electric fish (Zakon, 2012), evolution of resistance to lethal Na$_V$ channel toxins as observed in pufferfish and the blue-ringed octopus, and the adaptation to specific habitats, such as acid resistance in naked mole rats (Smith et al., 2011). Mature CNS neurons are equipped with isoforms, including Na$_V$1.2, Na$_V$1.1, and Na$_V$1.6, that were evolutionarily selected for fast conduction, clustering at axon initial segments and nodes of Ranvier, and are tailored with potassium channel kinetics for energy saving (Alle et al., 2009; Zakon, 2012). In contrast, polymodal nociceptors of the peripheral nervous system face extreme temperature changes and are abundant in the TTXs subtype Na$_V$1.7 and the two TTXr isoforms Na$_V$1.8 and Na$_V$1.9 (Waxman and Zamponi, 2014; Usoskin et al., 2015).

Downloaded from http://rupress.org/jgp/article-pdf/150/8/1125/1798734/jgp_201711786.pdf by guest on 09 February 2026

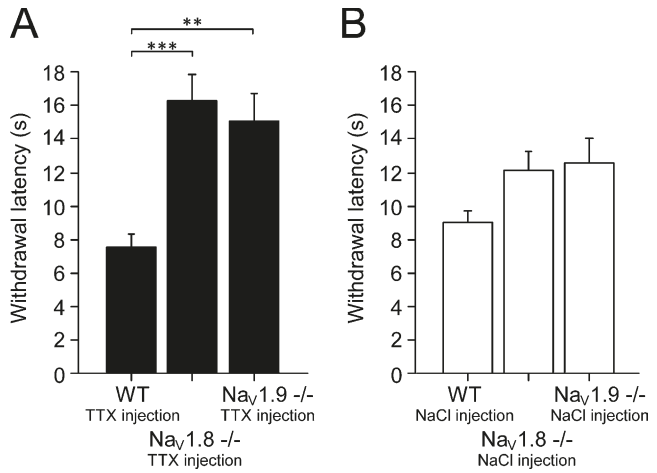

Figure 13. **Fast-gated TTXs Na_V channels reduce the heat pain threshold.** $Na_V1.8^{-/-}$, $Na_V1.9^{-/-}$, and littermate mice were subjected to heat pain threshold measurement with the plantar radiant heat test (Hargreave's apparatus). **(A)** After intraplantar administration of 3 µM TTX in a volume of 20 µl, the withdrawal latency was almost doubled in $Na_V1.8^{-/-}$ (***, P < 0.001) and $Na_V1.9^{-/-}$ (**, P < 0.01; *n* = 8 per group, both hindpaws were tested on two individual trials). **(B)** The same mice were measured before the application of TTX and showed a tendency to increased withdrawal latency (*n* = 8 per group), as previously observed (Akopian et al., 1999; Minett et al., 2014). Data are depicted as means ± SEM.

Our patch-clamp experiments identified a specialized physiological adaptive function of $Na_V1.9$ in the electrogenesis of nerve impulses at rising temperatures, where we found $Na_V1.9$'s activity to be substantially potentiated. Although both subtypes, $Na_V1.8$ and $Na_V1.9$, undergo a hyperpolarizing shift in $V_{1/2}$ of 3 and 4 mV in cultured DRG neurons when the temperature rises from 20°C to 30°C, remarkably only the $Na_V1.9$ isoform was able to sustain repetitive firing at 37°C. The striking difference between the temperature effects on both subtypes was the unexpected fourfold increase in conductance and peak current density mediated by $Na_V1.9$ upon warming of the perfusion solution from room temperature to normal skin temperature. In contrast, $Na_V1.8$ increased by only 1.7-fold. Although the $Na_V1.8$ current is variable and in some cells too large to be clamped, our recordings of the $Na_V1.9$ current measured at 30°C, and confirmed at 37°C and 43°C with CsF in the pipette solution, are in fact comparable in amplitude with $Na_V1.8$ at 10°C, this being the temperature where $Na_V1.8$ maintains its essential and unique function in cold nociceptors as the frost-resistant action potential ignition (Zimmermann et al., 2007).

Yet it was commonly accepted that $Na_V1.9$ contributes to the setting of the action potential threshold by producing a persistent current. By virtue of its ultra-slow activation and inactivation kinetics (at room temperature), $Na_V1.9$ was considered incapable of generating independent action potentials or of contributing to the rising phase of the action potential (Dib-Hajj et al., 1998, 2015; Rush et al., 2007). In contrast with this view, and in line with our voltage-clamp recordings, we succeeded in measuring action potentials in current-clamp mode at 37°C, but not at 20°C, in $Na_V1.8$-deficient cultured sensory neurons in the presence of TTX. Although the action potential shape at 20°C resembled the small graded depolarizations described by Renganathan et al. (2001), the action potentials at 37°C had a clear overshoot and a ~6-fold speeded kinetics compared with 20°C.

Several recent findings have implied a role for $Na_V1.9$ in acute and pathological cold pain (Leo et al., 2010; Leipold et al., 2015; Lolignier et al., 2015). The identified role of $Na_V1.9$ in these conditions is to amplify subthreshold depolarizations generated by cold transducer activation in a subpopulation of cold nociceptors devoid of TRPM8; our findings postulate an important functional contribution of $Na_V1.9$ channels to electrogenesis at rising temperatures. This implies that the function of $Na_V1.9$ is adapted to the entire temperature range and is therefore similar to $Na_V1.8$, which we revealed to be the crucial component of excitability >46°C and which is also the essential Na_V channel for electrogenesis at cold temperatures (Zimmermann et al., 2007). At lower temperatures, the membrane resistance of neurons increases and potassium conductance reduces, which requires less transduction current to trigger action potentials (Volgushev et al., 2000; Zimmermann et al., 2007). Although $Na_V1.9$-generated current densities are considerably smaller at 10°C, the persistent current remains and could become effective, because it is not counteracted by other ionic forces. In fact, in terminal nerve endings, it may help to reach the threshold of $Na_V1.8$-mediated action potentials, and even more under pathological conditions, where $Na_V1.9$ undergoes a gain of function, by either G protein–mediated sensitization or genetic mutation (Leipold et al., 2015; Lolignier et al., 2015). Nevertheless, our results predict that certain gain-of-function mutations in $Na_V1.9$ also result in warming-induced aggravation of pain.

In small-diameter nociceptive neurons, $Na_V1.8$ contributes most of the current to the upstroke of the action potential and triggers the entire action potential at low temperatures (Blair and Bean, 2002; Zimmermann et al., 2007). For $Na_V1.9$, the picture is less clear. This finding may point to different expression levels in these cells and potentially functionally distinct subgroups. Contactin is one molecule believed to influence $Na_V1.9$ ion channel density in the plasma membrane (Liu et al., 2001; Rush et al., 2005), and it has been reported that several auxiliary β-subunits of Na_V channels influence the kinetics of various current components (Huth et al., 2011; Zhang et al., 2013). This is why we speculate that the $Na_V1.9$ peak current component might also be a substrate of similar modulation, and this may sensitize its temperature sensitivity.

Our findings are in general accordance with the "dynamic" biophysical characteristics of $Na_V1.9$ observed in voltage-clamp recordings, where changes in current–voltage dependence to hyperpolarized potentials occur after whole-cell formation. These changes are sensitive to fluoride in the intracellular solution and can also be evoked by G protein–coupled receptor modulators, like some inflammatory agents (e.g., PGE2; Rush and Waxman, 2004; Baker, 2005; Ostman et al., 2008; Vanoye et al., 2013). For our recordings, we used both CsF and CsCl in the pipette solutions and obtained similar results for the potentiation of the $Na_V1.9$ current, although with CsCl, more stable current–voltage relationships are observed (Amaya et al., 2006). Nevertheless, there are more variables that need to be considered and contribute (possibly independently) to the $Na_V1.9$ current modulation. The separate regulation of the inactivating peak current

Downloaded from http://rupress.org/jgp/article-pdf/150/8/1125/1798734/jgp_201711786.pdf by guest on 09 February 2026

component and the persistent current and respective difference in the run-down of channel activity might indicate either a contamination of measurements with currents mediated by other ion channels (Coste et al., 2007) or the modulation of $Na_V1.9$ by distinct mediators present in neuronal cells. Voltage-gated calcium channels also contribute to a minor extent (compared with $Na_V1.8$ and TTXs Na_V channels) to action potential generation (Blair and Bean, 2002). We used 0.1 mM Cd^{2+} to block calcium channels. Although this does not exclude the possibility of some calcium channels being left unblocked, 0.1 mM Cd^{2+} indeed blocks the significant current component (Coste et al., 2007).

Interestingly, expression of $Na_V1.9$ has been verified on nociceptive $IB4^+$ small-diameter DRG neurons that express high levels of $Na_V1.9$, but no or subdetection levels of $Na_V1.8$, and which are predominantly heat-sensitive (Fang et al., 2006). $IB4^+$ neurons show relatively small heat responses (Stucky and Lewin, 1999). We suggest that this DRG subgroup corresponds to our S-type CMH fibers that require the $Na_V1.9$ isoform to generate responses to fast rising heat, and which should express reduced, but sufficient, levels of $Na_V1.8$ to generate action potentials at temperatures above 46°C.

Our threshold tracking experiments revealed that noxious heat–resistant nerve excitability is a distinctive feature of polymodal nociceptors, as it does not exist in cold nociceptors and, in contrast to cold, it requires several Na_V channel subtypes; in S-type CMH fibers, a TTXs Na_V channel subtype is crucial, and its lack becomes apparent above 34°C, where, even if $Na_V1.9$ and $Na_V1.8$ are active, excitability is lost in the presence of TTX. The absence of $Na_V1.9$ incapacitates the excitability to fast-rising heat but has little effect on the detection of slow-rising heat. Thus, in this fiber type, $Na_V1.9$ and a TTXs trigger, presumably the coexpressed $Na_V1.7$ (Usoskin et al., 2015), are sufficient to initiate heat-resistant sodium current up to ∼46°C. Above 46°C, $Na_V1.8$ becomes increasingly relevant to generate the heat-resistant action potential, which is illustrated by our excitability tracking in $Na_V1.8^{-/-}$. In line with this finding, its absence has little effect on withdrawal thresholds in animals. Nevertheless, in L-type CMH fibers, we observed that the TTXs current contribution is much smaller, and likely both TTXr channels replace the TTXs action potential generator with increasing temperature. This is because a lack of either $Na_V1.9$ or $Na_V1.8$ reduces the heat response to a fast heat ramp for temperatures above ∼44°C. Evidently, in both CMH fiber types, $Na_V1.9$'s functional significance increases with temperature, alongside the speeding of its kinetics and the increase of its peak current amplitude. This is illustrated by the huge effect of $Na_V1.9$ on the voltage threshold with rising temperatures, with this becoming apparent by the removal of the TTXs current component in $Na_V1.8$-deficient DRGs. Previous studies have not observed this feature of $Na_V1.9$ (Priest et al., 2005; Leipold et al., 2015), because apparently $Na_V1.9$ and $Na_V1.8$ in combination are able to maintain the threshold to a large extent, even without the fast-gated TTXs channels, as our WT recordings (in Fig. 7) demonstrated.

It is yet unclear which physiological function S- and L-type heat-sensing pathways serve. They are seemingly not equipped with different sets of heat transducers, as skin-nerve recordings from combinations of double knockouts of the crucial heat transducer trio TRPA1, TRPM3, and TRPV1 have revealed (Vandewauw et al., 2018). They could have emerged during evolution as redundant and serve as a backup for each other. Lack of function to one of the Na_V channel subtypes, $Na_V1.8$ or $Na_V1.9$, affects their heat responsiveness rather differently and would not disable detection of damaging heat. In fact, lack of either TTXr channel in the absence of the TTXs trigger leaves the animal with a prolonged withdrawal latency, but still allows protection from damaging heat (Akopian et al., 1999; Minett et al., 2014). In $Na_V1.8^{-/-}$, the prolonged withdrawal response to infrared radiant heat seems caused by encoding deficits in L-type CMHs, because S-type CMHs are affected only at temperatures beyond the heat pain threshold. In $Na_V1.9$-deficient mice, the prolongation of the withdrawal response is caused by incapacitated S-type CMHs and remains compensated for by L-type CMHs, which still activate at the same heat threshold, and their heat response is rising with a faster slope. After the injection of TTX, the withdrawal response prolongs by ∼50% in both genotypes. In $Na_V1.8^{-/-}$, this effect can be attributed to a reduced function of TTX-blocked S-type CMHs, whereas in $Na_V1.9^{-/-}$, it is caused by the reduced L-type response, which reduces the dynamic range and leaves $Na_V1.8$ as the only Na_V channel. Because this type of TTX application certainly leaves some TTXs channels unblocked as a result of inhomogeneous tissue distribution, it leaves open the question whether $Na_V1.8$ alone may sustain a heat withdrawal reaction in the absence of all other Na_V channel subtypes. The different high- and low-frequency encoded heat responses may also be required to allow the detection of both slowly rising (L-type) and fast-rising heat (S-type), because in contrast to L-type CMHs, S-type CMHs suffer adaptation during slowly rising heat ramps and produce only few or no action potentials. Other than that, the existence of two lines of heat fiber types may also exist to allow a more sophisticated neuronal computation of sensory information in the spinal cord (McCoy et al., 2013), leading to a better fine-tuning of temperature sensitivity in general.

Acknowledgments

The authors acknowledge Christian Alzheimer and Fang Zheng at the Department of Physiology and Pathophysiology at FAU for their contributions to an earlier version of this manuscript. The authors also thank David Clapham at the Janelia Research Campus for insightful discussions of the patch clamp recordings. Iwona Izydorkzyck provided excellent support with the DRG cultures, Jana Schramm bred and genotyped the transgenic mice, and Hana Starobova is acknowledged for assistance with the behavioral experiments (blinded the groups and injected the TTX).

This study was funded by the German Research Foundation (Zi 1171/2-1, Zi 1171/3-1), the Marohn- and Erika-Giehrl Foundations at the Friedrich-Alexander University Erlangen-Nürnberg, and the Czech Science Foundation (15-15839S).

The authors declare no competing financial interests.

Author contributions: F. Touska planned, performed, and analyzed the patch-clamp and behavioral experiments and designed the figures. B. Turnquist developed and implemented the threshold tracking script and performed simulations and experiments. K. Zimmermann planned, performed, and analyzed the

Downloaded from http://rupress.org/jgp/article-pdf/150/8/1125/1798734/jgp_201711786.pdf by guest on 09 February 2026

extracellular recordings and designed the figures. F. Touska and K. Zimmermann wrote the draft, and all authors discussed the results and contributed to the final manuscript. A. Leffler and K. Zimmermann conceived the idea, and V. Vlachova and P.W. Reeh helped supervise the project.

Kenton J. Swartz served as editor.

Submitted: 15 March 2017
Revised: 31 December 2017
Accepted: 29 May 2018

References

Akopian, A.N., V. Souslova, S. England, K. Okuse, N. Ogata, J. Ure, A. Smith, B.J. Kerr, S.B. McMahon, S. Boyce, et al. 1999. The tetrodotoxin-resistant sodium channel SNS has a specialized function in pain pathways. *Nat. Neurosci.* 2:541–548. https://doi.org/10.1038/9195

Alle, H., A. Roth, and J.R. Geiger. 2009. Energy-efficient action potentials in hippocampal mossy fibers. *Science.* 325:1405–1408. https://doi.org/10.1126/science.1174331

Amaya, F., H. Wang, M. Costigan, A.J. Allchorne, J.P. Hatcher, J. Egerton, T. Stean, V. Morisset, D. Grose, M.J. Gunthorpe, et al. 2006. The voltage-gated sodium channel Na(v)1.9 is an effector of peripheral inflammatory pain hypersensitivity. *J. Neurosci.* 26:12852–12860. https://doi.org/10.1523/JNEUROSCI.4015-06.2006

Baker, M.D. 2005. Protein kinase C mediates up-regulation of tetrodotoxin-resistant, persistent Na+ current in rat and mouse sensory neurones. *J. Physiol.* 567:851–867. https://doi.org/10.1113/jphysiol.2005.089771

Bessou, P., and E.R. Perl. 1969. Response of cutaneous sensory units with unmyelinated fibers to noxious stimuli. *J. Neurophysiol.* 32:1025–1043. https://doi.org/10.1152/jn.1969.32.6.1025

Blair, N.T., and B.P. Bean. 2002. Roles of tetrodotoxin (TTX)-sensitive Na+ current, TTX-resistant Na+ current, and Ca2+ current in the action potentials of nociceptive sensory neurons. *J. Neurosci.* 22:10277–10290. https://doi.org/10.1523/JNEUROSCI.22-23-10277.2002

Bretag, A.H. 1969. Synthetic interstitial fluid for isolated mammalian tissue. *Life Sci.* 8:319–329. https://doi.org/10.1016/0024-3205(69)90283-5

Caterina, M.J., A. Leffler, A.B. Malmberg, W.J. Martin, J. Trafton, K.R. Petersen-Zeitz, M. Koltzenburg, A.I. Basbaum, and D. Julius. 2000. Impaired nociception and pain sensation in mice lacking the capsaicin receptor. *Science.* 288:306–313. https://doi.org/10.1126/science.288.5464.306

Coste, B., N. Osorio, F. Padilla, M. Crest, and P. Delmas. 2004. Gating and modulation of presumptive NaV1.9 channels in enteric and spinal sensory neurons. *Mol. Cell. Neurosci.* 26:123–134. https://doi.org/10.1016/j.mcn.2004.01.015

Coste, B., M. Crest, and P. Delmas. 2007. Pharmacological dissection and distribution of NaN/Nav1.9, T-type Ca^{2+} currents, and mechanically activated cation currents in different populations of DRG neurons. *J. Gen. Physiol.* 129:57–77. https://doi.org/10.1085/jgp.200609665

Cox, J.J., F. Reimann, A.K. Nicholas, G. Thornton, E. Roberts, K. Springell, G. Karbani, H. Jafri, J. Mannan, Y. Raashid, et al. 2006. An SCN9A channelopathy causes congenital inability to experience pain. *Nature.* 444:894–898. https://doi.org/10.1038/nature05413

Cummins, T.R., S.D. Dib-Hajj, J.A. Black, A.N. Akopian, J.N. Wood, and S.G. Waxman. 1999. A novel persistent tetrodotoxin-resistant sodium current in SNS-null and wild-type small primary sensory neurons. *J. Neurosci.* 19:RC43. https://doi.org/10.1523/JNEUROSCI.19-24-j0001.1999

Dib-Hajj, S.D., L. Tyrrell, J.A. Black, and S.G. Waxman. 1998. NaN, a novel voltage-gated Na channel, is expressed preferentially in peripheral sensory neurons and down-regulated after axotomy. *Proc. Natl. Acad. Sci. USA.* 95:8963–8968. https://doi.org/10.1073/pnas.95.15.8963

Dib-Hajj, S., J.A. Black, T.R. Cummins, and S.G. Waxman. 2002. NaN/Nav1.9: A sodium channel with unique properties. *Trends Neurosci.* 25:253–259. https://doi.org/10.1016/S0166-2236(02)02150-1

Dib-Hajj, S.D., J.A. Black, and S.G. Waxman. 2015. NaV1.9: A sodium channel linked to human pain. *Nat. Rev. Neurosci.* 16:511–519. https://doi.org/10.1038/nrn3977

Dittert, I., J. Benedikt, L. Vyklický, K. Zimmermann, P.W. Reeh, and V. Vlachová. 2006. Improved superfusion technique for rapid cooling or heating of cultured cells under patch-clamp conditions. *J. Neurosci. Methods.* 151:178–185. https://doi.org/10.1016/j.jneumeth.2005.07.005

Enyedi, P., and G. Czirják. 2010. Molecular background of leak K+ currents: Two-pore domain potassium channels. *Physiol. Rev.* 90:559–605. https://doi.org/10.1152/physrev.00029.2009

Fang, X., L. Djouhri, S. McMullan, C. Berry, S.G. Waxman, K. Okuse, and S.N. Lawson. 2006. Intense isolectin-B4 binding in rat dorsal root ganglion neurons distinguishes C-fiber nociceptors with broad action potentials and high Nav1.9 expression. *J. Neurosci.* 26:7281–7292. https://doi.org/10.1523/JNEUROSCI.1072-06.2006

Fujii, T., and Y. Ibata. 1982. Effects of heating on electrical activities of guinea pig olfactory cortical slices. *Pflugers Arch.* 392:257–260. https://doi.org/10.1007/BF00584306

Griffin, J.D., and J.A. Boulant. 1995. Temperature effects on membrane potential and input resistance in rat hypothalamic neurones. *J. Physiol.* 488:407–418. https://doi.org/10.1113/jphysiol.1995.sp020975

Hampl, M., E. Eberhardt, A.O. O'Reilly, and A. Lampert. 2016. Sodium channel slow inactivation interferes with open channel block. *Sci. Rep.* 6:25974. https://doi.org/10.1038/srep25974

Hodgkin, A.L., and B. Katz. 1949. The effect of temperature on the electrical activity of the giant axon of the squid. *J. Physiol.* 109:240–249. https://doi.org/10.1113/jphysiol.1949.sp004388

Huth, T., A. Rittger, P. Saftig, and C. Alzheimer. 2011. β-Site APP-cleaving enzyme 1 (BACE1) cleaves cerebellar Na+ channel β4-subunit and promotes Purkinje cell firing by slowing the decay of resurgent Na+ current. *Pflugers Arch.* 461:355–371. https://doi.org/10.1007/s00424-010-0913-2

Jo, S., and B.P. Bean. 2011. Inhibition of neuronal voltage-gated sodium channels by brilliant blue G. *Mol. Pharmacol.* 80:247–257. https://doi.org/10.1124/mol.110.070276

Leipold, E., A. Hanson-Kahn, M. Frick, P. Gong, J.A. Bernstein, M. Voigt, I. Katona, R. Oliver Goral, J. Altmüller, P. Nürnberg, et al. 2015. Cold-aggravated pain in humans caused by a hyperactive NaV1.9 channel mutant. *Nat. Commun.* 6:10049. https://doi.org/10.1038/ncomms10049

Leo, S., R. D'Hooge, and T. Meert. 2010. Exploring the role of nociceptor-specific sodium channels in pain transmission using Nav1.8 and Nav1.9 knockout mice. *Behav. Brain Res.* 208:149–157. https://doi.org/10.1016/j.bbr.2009.11.023

Liu, C.J., S.D. Dib-Hajj, J.A. Black, J. Greenwood, Z. Lian, and S.G. Waxman. 2001. Direct interaction with contactin targets voltage-gated sodium channel Na(v)1.9/NaN to the cell membrane. *J. Biol. Chem.* 276:46553–46561. https://doi.org/10.1074/jbc.M108699200

Lolignier, S., C. Bonnet, C. Gaudioso, J. Noël, J. Ruel, M. Amsalem, J. Ferrier, L. Rodat-Despoix, V. Bouvier, Y. Aissouni, et al. 2015. The Nav1.9 channel is a key determinant of cold pain sensation and cold allodynia. *Cell Reports.* 11:1067–1078. https://doi.org/10.1016/j.celrep.2015.04.027

Lyfenko, A., V. Vlachová, L. Vyklický, I. Dittert, M. Kress, and P.W. Reeh. 2002. The effects of excessive heat on heat-activated membrane currents in cultured dorsal root ganglia neurons from neonatal rat. *Pain.* 95:207–214. https://doi.org/10.1016/S0304-3959(01)00401-8

Matsutomi, T., C. Nakamoto, T. Zheng, J. Kakimura, and N. Ogata. 2006. Multiple types of Na(+) currents mediate action potential electrogenesis in small neurons of mouse dorsal root ganglia. *Pflugers Arch.* 453:83–96. https://doi.org/10.1007/s00424-006-0104-3

McCoy, E.S., B. Taylor-Blake, S.E. Street, A.L. Pribisko, J. Zheng, and M.J. Zylka. 2013. Peptidergic CGRPα primary sensory neurons encode heat and itch and tonically suppress sensitivity to cold. *Neuron.* 78:138–151. https://doi.org/10.1016/j.neuron.2013.01.030

Minett, M.S., N. Eijkelkamp, and J.N. Wood. 2014. Significant determinants of mouse pain behaviour. *PLoS One.* 9:e104458. https://doi.org/10.1371/journal.pone.0104458

Nevo, E. 2011. Evolution under environmental stress at macro- and microscales. *Genome Biol. Evol.* 3:1039–1052. https://doi.org/10.1093/gbe/evr052

Ostman, J.A., M.A. Nassar, J.N. Wood, and M.D. Baker. 2008. GTP up-regulated persistent Na+ current and enhanced nociceptor excitability require NaV1.9. *J. Physiol.* 586:1077–1087. https://doi.org/10.1113/jphysiol.2007.147942

Priest, B.T., B.A. Murphy, J.A. Lindia, C. Diaz, C. Abbadie, A.M. Ritter, P. Liberator, L.M. Iyer, S.F. Kash, M.G. Kohler, et al. 2005. Contribution of the tetrodotoxin-resistant voltage-gated sodium channel NaV1.9 to sensory transmission and nociceptive behavior. *Proc. Natl. Acad. Sci. USA.* 102:9382–9387. https://doi.org/10.1073/pnas.0501549102

Downloaded from http://rupress.org/jgp/article-pdf/150/8/1125/1798734/jgp_201711786.pdf by guest on 09 February 2026

Renganathan, M., T.R. Cummins, and S.G. Waxman. 2001. Contribution of Na(v)1.8 sodium channels to action potential electrogenesis in DRG neurons. *J. Neurophysiol.* 86:629–640. https://doi.org/10.1152/jn.2001.86.2.629

Rogers, M., N. Zidar, D. Kikelj, and R.W. Kirby. 2016. Characterization of endogenous sodium channels in the ND7-23 neuroblastoma cell line: Implications for use as a heterologous ion channel expression system suitable for automated patch clamp screening. *Assay Drug Dev. Technol.* 14:109–130. https://doi.org/10.1089/adt.2016.704

Rugiero, F., M. Mistry, D. Sage, J.A. Black, S.G. Waxman, M. Crest, N. Clerc, P. Delmas, and M. Gola. 2003. Selective expression of a persistent tetrodotoxin-resistant Na+ current and NaV1.9 subunit in myenteric sensory neurons. *J. Neurosci.* 23:2715–2725. https://doi.org/10.1523/JNEUROSCI.23-07-02715.2003

Rush, A.M., and S.G. Waxman. 2004. PGE2 increases the tetrodotoxin-resistant Nav1.9 sodium current in mouse DRG neurons via G-proteins. *Brain Res.* 1023:264–271. https://doi.org/10.1016/j.brainres.2004.07.042

Rush, A.M., M.J. Craner, T. Kageyama, S.D. Dib-Hajj, S.G. Waxman, and B. Ranscht. 2005. Contactin regulates the current density and axonal expression of tetrodotoxin-resistant but not tetrodotoxin-sensitive sodium channels in DRG neurons. *Eur. J. Neurosci.* 22:39–49. https://doi.org/10.1111/j.1460-9568.2005.04186.x

Rush, A.M., T.R. Cummins, and S.G. Waxman. 2007. Multiple sodium channels and their roles in electrogenesis within dorsal root ganglion neurons. *J. Physiol.* 579:1–14. https://doi.org/10.1113/jphysiol.2006.121483

Shen, K.F., and P.A. Schwartzkroin. 1988. Effects of temperature alterations on population and cellular activities in hippocampal slices from mature and immature rabbit. *Brain Res.* 475:305–316. https://doi.org/10.1016/0006-8993(88)90619-1

Smith, E.S., D. Omerbašić, S.G. Lechner, G. Anirudhan, L. Lapatsina, and G.R. Lewin. 2011. The molecular basis of acid insensitivity in the African naked mole-rat. *Science.* 334:1557–1560. https://doi.org/10.1126/science.1213760

St Pierre, M., P.W. Reeh, and K. Zimmermann. 2009. Differential effects of TRPV channel block on polymodal activation of rat cutaneous nociceptors in vitro. *Exp. Brain Res.* 196:31–44. https://doi.org/10.1007/s00221-009-1808-3

Stucky, C.L., and G.R. Lewin. 1999. Isolectin B(4)-positive and -negative nociceptors are functionally distinct. *J. Neurosci.* 19:6497–6505. https://doi.org/10.1523/JNEUROSCI.19-15-06497.1999

Tate, S., S. Benn, C. Hick, D. Trezise, V. John, R.J. Mannion, M. Costigan, C. Plumpton, D. Grose, Z. Gladwell, et al. 1998. Two sodium channels contribute to the TTX-R sodium current in primary sensory neurons. *Nat. Neurosci.* 1:653–655. https://doi.org/10.1038/3652

Usoskin, D., A. Furlan, S. Islam, H. Abdo, P. Lönnerberg, D. Lou, J. Hjerling-Leffler, J. Haeggström, O. Kharchenko, P.V. Kharchenko, et al. 2015. Unbiased classification of sensory neuron types by large-scale single-cell RNA sequencing. *Nat. Neurosci.* 18:145–153. https://doi.org/10.1038/nn.3881

Vandewauw, I., K. De Clercq, M. Mulier, K. Held, S. Pinto, N. Van Ranst, A. Segal, T. Voet, R. Vennekens, K. Zimmermann, et al. 2018. A TRP channel trio mediates acute noxious heat sensing. *Nature.* 555:662–666. https://doi.org/10.1038/nature26137

Vanoye, C.G., J.D. Kunic, G.R. Ehring, and A.L. George Jr. 2013. Mechanism of sodium channel $Na_V1.9$ potentiation by G-protein signaling. *J. Gen. Physiol.* 141:193–202. https://doi.org/10.1085/jgp.201210919

Vetter, I., A. Hein, S. Sattler, S. Hessler, F. Touska, E. Bressan, A. Parra, U. Hager, A. Leffler, S. Boukalova, et al. 2013. Amplified cold transduction in native nociceptors by M-channel inhibition. *J. Neurosci.* 33:16627–16641. https://doi.org/10.1523/JNEUROSCI.1473-13.2013

Volgushev, M., T.R. Vidyasagar, M. Chistiakova, T. Yousef, and U.T. Eysel. 2000. Membrane properties and spike generation in rat visual cortical cells during reversible cooling. *J. Physiol.* 522:59–76. https://doi.org/10.1111/j.1469-7793.2000.0059m.x

Vyklický, L., V. Vlachová, Z. Vitásková, I. Dittert, M. Kabát, and R.K. Orkand. 1999. Temperature coefficient of membrane currents induced by noxious heat in sensory neurones in the rat. *J. Physiol.* 517:181–192. https://doi.org/10.1111/j.1469-7793.1999.0181z.x

Waxman, S.G., and G.W. Zamponi. 2014. Regulating excitability of peripheral afferents: Emerging ion channel targets. *Nat. Neurosci.* 17:153–163. https://doi.org/10.1038/nn.3602

Winter, Z., P. Gruschwitz, S. Eger, F. Touska, and K. Zimmermann. 2017. Cold temperature encoding by cutaneous TRPA1 and TRPM8-carrying fibers in the mouse. *Front. Mol. Neurosci.* 10:209. https://doi.org/10.3389/fnmol.2017.00209

Zakon, H.H. 2012. Adaptive evolution of voltage-gated sodium channels: The first 800 million years. *Proc. Natl. Acad. Sci. USA.* 109(Suppl 1):10619–10625. https://doi.org/10.1073/pnas.1201884109

Zhang, M.M., M.J. Wilson, L. Azam, J. Gajewiak, J.E. Rivier, G. Bulaj, B.M. Olivera, and D. Yoshikami. 2013. Co-expression of Na(V)β subunits alters the kinetics of inhibition of voltage-gated sodium channels by pore-blocking μ-conotoxins. *Br. J. Pharmacol.* 168:1597–1610. https://doi.org/10.1111/bph.12051

Zimmermann, K., A. Leffler, M.M. Fischer, K. Messlinger, C. Nau, and P.W. Reeh. 2005. The TRPV1/2/3 activator 2-aminoethoxydiphenyl borate sensitizes native nociceptive neurons to heat in wildtype but not TRPV1 deficient mice. *Neuroscience.* 135:1277–1284. https://doi.org/10.1016/j.neuroscience.2005.07.018

Zimmermann, K., A. Leffler, A. Babes, C.M. Cendan, R.W. Carr, J. Kobayashi, C. Nau, J.N. Wood, and P.W. Reeh. 2007. Sensory neuron sodium channel Nav1.8 is essential for pain at low temperatures. *Nature.* 447:855–858. https://doi.org/10.1038/nature05880

Zimmermann, K., A. Hein, U. Hager, J.S. Kaczmarek, B.P. Turnquist, D.E. Clapham, and P.W. Reeh. 2009. Phenotyping sensory nerve endings in vitro in the mouse. *Nat. Protoc.* 4:174–196. https://doi.org/10.1038/nprot.2008.223

Zimmermann, K., J.K. Lennerz, A. Hein, A.S. Link, J.S. Kaczmarek, M. Delling, S. Uysal, J.D. Pfeifer, A. Riccio, and D.E. Clapham. 2011. Transient receptor potential cation channel, subfamily C, member 5 (TRPC5) is a cold-transducer in the peripheral nervous system. *Proc. Natl. Acad. Sci. USA.* 108:18114–18119. https://doi.org/10.1073/pnas.1115387108

Downloaded from http://rupress.org/jgp/article-pdf/150/8/1125/1798734/jgp_201711786.pdf by guest on 09 February 2026